Engineering Structures 304 (2024) 117562

Contents lists available at ScienceDirect

Engineering Structures

journal homepage: www.elsevier.com/locate/engstruct

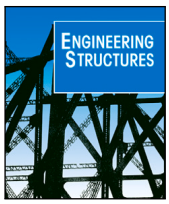

Load distribution and passive confinement in reinforced concrete: Development of a mechanical model

Clemens Proksch-Weilguni *, Marion Decker, Johann Kollegger

Institute of Structural Engineering, TU Wien, Karlsplatz 13, Vienna, 1040, Austria

ARTICLE INFO

Keywords:
Mechanical model
Reinforced concrete
Geometric confinement
Passive confinement
Load transfer zones
Load-bearing capacity
Experimental investigations

ABSTRACT

Understanding the load-bearing behavior of joints between precast concrete elements under compression is of great interest for practical applications, such as tunnel linings. Based on a literature review a research gap on the interaction of a concentrated load introduction (causing geometric confinement) and transverse reinforcement (causing passive confinement) is identified in this paper. This lack of knowledge was addressed in 26 experimental tests at the Institute of Structural Engineering at TU Wien. In these tests the load introduction area, the reinforcement ratio and the load introduction material were varied. Thereby it was confirmed that the confining effect of the transverse reinforcement has a significant influence on the load-bearing behavior. With the experimental results, a new mechanical model including a semi-empirical component for predicting the load-bearing capacity of load transfer zones with geometric and passive confinement was verified and afterwards validated with data from literature. The developed model provides a solution to describe the interaction of geometric and passive confinement based on simple mechanical considerations. In comparison to the existing models implemented in current design codes, where no interaction between geometric and passive confinement is taken into account, a more efficient design for load transfer zones will be enabled.

1. Introduction

1.1. Motivation and historical background

The transfer of compressive stresses between precast concrete elements is of great importance in practical applications such as in tunnel constructions. There, the stresses have to be transferred from one tunnel segment to another via a contact surface. The area of the contact surface with a reduced cross section and the adjacent part of the segments, where a discontinuous load distribution occurs, can be designated as the load transfer zone. As numerous identical prefabricated tunnel segments are required for the construction of a tunnel structure, there is a great interest in better understanding the load-bearing behavior of these load transfer zones.

According to Saint-Venant's principle [2] a concentrated force, that is applied to a limited contact area A_{c0}, distributes over the height h, which is equal to the decisive width d (outlined in Fig. 1), in the plane parallel to the stress distribution. In this context the term *partially loaded area* is the most commonly used in the field of structural engineering. To describe the different mechanical effects, which are related to the topic of partially loaded areas, more precisely, the authors use the terminology *geometric* and *passive confinement*. The term *load transfer zone* is used explicitly for the situation when stresses are transferred between two concrete elements instead of using a steel plate for load application.

The increase of the uniaxial concrete strength f_c, which is caused through load distribution is referred to the *geometric confinement*, since the geometrical situation of the concrete element is crucial for the confinement (examples are shown in Fig. 1a and Fig. 1b). The definition of geometric confinement is based on the circumstance, that there is no lateral strain, initialized by the axial force, needed (similar to active confinement) in contrast to passive confinement. This terminology was used e.g. in Markić et al. [3,4] to describe the load-bearing behavior of reinforced concrete elements with concentrated load introduction. First experiments investigating confinement caused by concentrated load introduction were performed by Bauschinger [5] in 1876 and resulted in the *cubic root equation* describing the increase of the uniaxial strength of stone blocks. The empirically derived *square root equation*, which is still widely used in current standards (e.g. EN 1992-1-1 [6], fib Model Code 2010 [7] and SIA 262 [8]) is the most common approach to capture the effect of geometric confinement and was presented in the dissertation of Spieth [9] in 1959.

Passive confinement in general is caused by the impediment of lateral expansion of the loaded concrete elements by enclosed steel tubes, fiber-reinforced polymer (FRP) wrapping, a stiff steel plate used for

* Corresponding author.
E-mail address: clemens.proksch-weilguni@tuwien.ac.at (C. Proksch-Weilguni).

https://doi.org/10.1016/j.engstruct.2024.117562
Received 3 July 2023; Received in revised form 12 December 2023; Accepted 21 January 2024
Available online 9 February 2024

Nomenclature

A_c	Cross-sectional area of the concrete element
A_{c0}	Area of the contact surface
A_{c1}	Area of the concrete element available for load distribution
A_{cc}	Confined concrete area
$A_{cc.e}$	Effective confined concrete area
A_s	Cross-sectional area of a transverse reinforcement layer (for a cylindrical hoop $A_s = 2(\varnothing^2\pi/4)$)
E_{cm}	Secant modulus of elasticity of concrete
F	Axial force
$F_{cal.GPC0}$	Load-bearing capacity according the GPC-model in section 0–0
$F_{cal.GPC1}$	Load-bearing capacity according the GPC-model in section 1–1
F_{cal}	Calculated load-bearing capacity
F_{cm}	Load-bearing capacity component caused by the uniaxial concrete strength
$F_{cal.EC2}$	Load-bearing capacity according to EC2-draft
$F_{cal.EC2conf}$	Load-bearing capacity according to the EC2-draft [1]
F_{exp}	Experimentally determined load-bearing capacity
F_t	Resulting tensile force in the tensile ring
H	Height of the test specimen
R_0	Region that defines the reinforcement layers which are not allowed to be considered for assigning tensile forces of the tension ring
R_1	Region that defines the reinforcement layers which are allowed to be considered for assigning tensile forces of the tension ring
R^2	coefficient of determination
b	Dimension of the concrete element in direction of the thickness
b_0	Dimension of the contact surface in direction of the thickness
b_c	Dimension of a rectangular shaped confined concrete core at confinement reinforcement
d	Dimension of the concrete element in direction of the width
d_0	Dimension of the contact surface in direction of the width
d_c	Width/Diameter of the confined concrete core at confinement reinforcement
f_c	Concrete compressive strength
f_{cm}	Mean concrete cylinder compressive strength
$f_{cm,cube}$	Mean concrete cube compressive strength
f_{ctm}	Mean tensile strength of concrete
f_y	Yield strength of reinforcement
f_{ym}	Mean yield strength of reinforcement
h	Height of the load distribution zone
$k_{conf.b}$	Effectiveness factor depending on the reinforcement layout according to the EC2-draft [1]
$k_{conf.s}$	Effectiveness factor depending on the reinforcement layout according to the EC2-draft [1]
n_0	number of reinforcement layers located in R_0
n_1	number of reinforcement layers located in R_1
n_{sp}	Number of transverse reinforcement layers which are considered for covering the transverse tensile forces
s_c	Spacing between the transverse reinforcement bars in the discontinuity region
$s_{c.cont}$	Spacing between the contact surface and the first transverse reinforcement layer adjacent to it
x_{sp}	Distance between the compression ring and the resulting tensile force in the tension ring depending on the reinforcement layout
ΔF_c	Load-bearing capacity component caused by geometric confinement
$\Delta F_{s.cc}$	Load-bearing capacity component caused by passive confinement
Δf_c	Compressive strength increase due to load distribution in the concrete
$\Delta f_{s.cc}$	Compressive strength increase due to steel confined concrete
$\Delta\sigma_{s.cc}$	Compressive strength increase due to steel confined concrete evenly distributed over the contact surface A_{c0}
$\varnothing$	Diameter of a reinforcement bar
ε_u	Ultimate strain when reaching the peak load
ρ	Volumetric reinforcement ratio
σ_{c0}	Compressive stress in the contact surface
$\sigma_{c0.exp}$	Experimentally determined compressive stress in the contact surface
σ_{cc}	Transverse compressive stress in concrete generated by transverse reinforcement
ν_{part}	Factor which builds an upper limit for $\sqrt{\frac{A_{c1}}{A_{c0}}}$
ω	Mechanical reinforcement ratio

load introduction, the unloaded concrete outside of the area of the concentrated load introduction or transverse reinforcement located inside the concrete. Further it has to be distinguished between pre-cracking passive confinement (e.g. caused by the unloaded concrete outside of the area of the concentrated load introduction), which relies on the tensile strength of concrete, and post-cracking passive confinement (e.g. caused by transverse reinforcement) which needs large lateral deformations to be activated. When reaching the peak load in reinforced concrete elements only post-cracking passive confinement and geometric confinement are relevant for the load-bearing behavior. For this reason only these two effects are investigated in this publication and post-cracking passive confinement will be simplified with the term passive confinement. Examples for passive confinement caused by reinforcement are shown in Fig. 1c and Fig. 1d. The effect has already been investigated in depth for columns, in particular the ductile behavior when exposed to seismic loads [10]. The first investigation regarding passive confinement caused by spiral reinforcement goes back to Richart et al. in 1929 [11]. Later, in 1988, Mander et al. [12] published a design approach for passive confinement in circular and rectangular shaped concrete elements, with its fundamentals still used in current design codes [1,7] and the newly presented model.

In addition to geometric and passive confinement the term *active confinement* is generally used for external forces e.g. applied circumferential prestressing or lateral water pressure which is not relevant for this research work.

1.2. Research gap

Researchers have been investigating the behavior of confinement in concrete for almost 150 years, with the first experiments conducted by

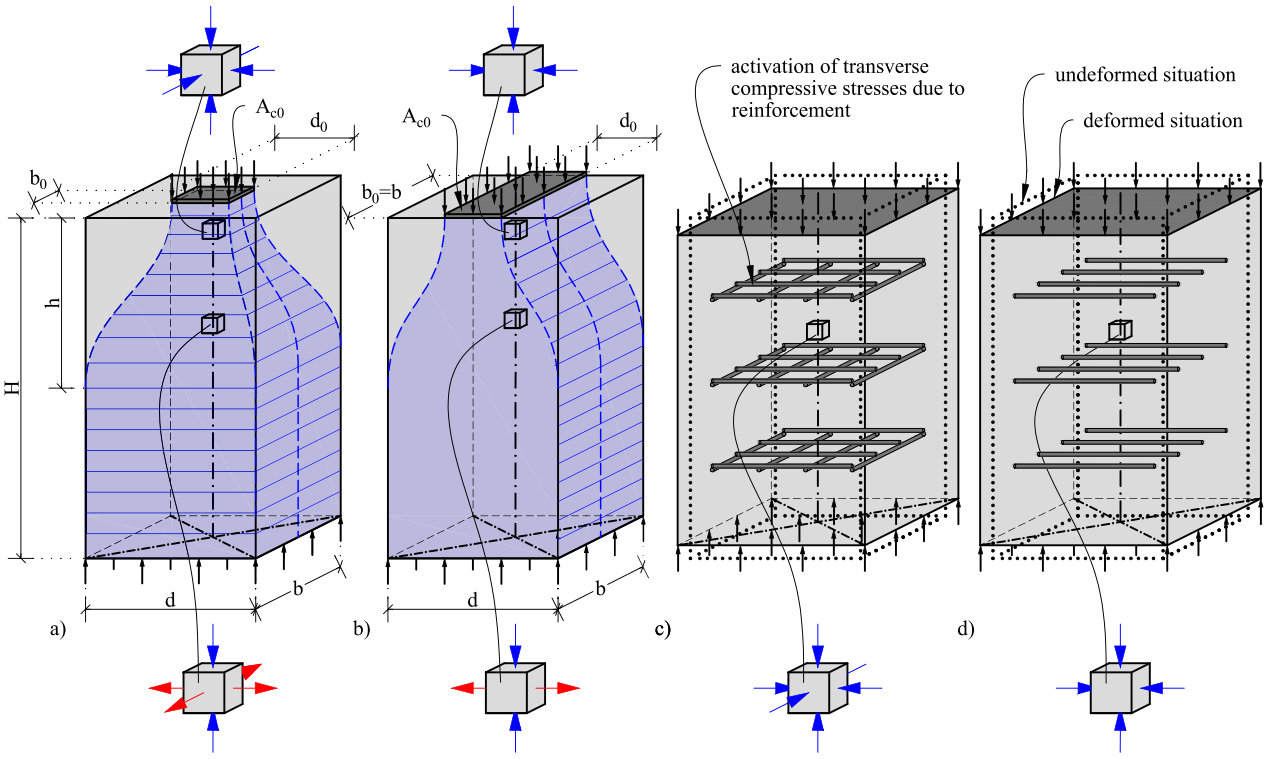

Fig. 1. Compressive stress states caused by geometric confinement: (a) spatial case, (b) plane case; Stress states caused by passive confinement: (c) spatial case, (d) plane case. (For interpretation of the references to color in this figure, the reader is referred to the web version of this article.).

Bauschinger [5] in 1876. The state of the art in the future European design code [1] of concentrated load introductions with the square root equation is based on five empirical tests of unreinforced concrete cylinders by Spieth (1959) [9,13]. The approach has its limitations when it comes to describing the behavior of highly reinforced concrete elements. Despite the great progress made in regard to understanding the mechanical behavior of confined concrete, the following research gaps remained which can be partly bridged by the research presented within this publication:

- An increase in ultimate load due to additional transverse reinforcement is neither considered in the square root approach according to the current EC2 [6] and its application in the German guideline for designing tunnel segments (DAUB [14]) nor in the new EC2-draft [1] according to Section 2.3.1. Therein the transverse reinforcement only forms a lower bound to prevent brittle tensile failure. In the combined models of Wichers [15], Wurm & Daschner [16] and Niyogi [17], the transverse reinforcement is considered as an empirically determined additive term with strong restrictions on its application (the model of Wichers [15], for example, is limited to transverse reinforcement ratios of $\rho = 1\,\%$. Therefore the geometric reinforcement ratio $\rho = A_s/(s_c \cdot d_c)$ in the presented experimental investigations varies from $0\,\%$ to $2.57\,\%$.
- The design models in literature [9,15,16] were developed for a wide range of load concentration ratios with A_{c1}/A_{c0} ranging from 1 to 100. When specifying it for longitudinal joints of tunnel segments with either centric or eccentric loading, the ratio ranges from 1.44 to 2.5 or 1.44 to 12.5, respectively [18]. Within the presented experimental campaign the focus is set on the lower spectrum with A_{c1}/A_{c0} from 1.0 to 4.0.
- In literature most experiments [9,16,17,19–21] regarding the load-bearing capacity of geometric confinement were carried out using steel plates (which causes additional passive confinement) for load introduction. However, in practical applications, like the longitudinal joint between two tunnel segments, the load is transferred directly between two concrete surfaces. Compared to this, the influence of the transverse strain restraint due to a load introduction surface made of steel is investigated in this paper.

When determining the load-bearing capacity of longitudinal segment joints, there is a considerable need for fundamental research due to the specific boundary conditions of small ratios of A_{c1}/A_{c0}, high transverse reinforcement ratios and concrete–concrete (c–c) load introduction.

2. Mechanical principles

In the case of concentrated load introduction with transverse reinforcement geometric and passive confinement may occur simultaneously, which is illustrated in Fig. 2a. Since the geometry of cylinders simplifies the mechanical principals and the experimental investigations, further investigations in this publication will be based on cylindrical concrete elements. Existing models in the design codes [1,7,8] and in literature [12,22] provide solutions for predicting the confinement effects on circular and rectangular shaped concrete elements, which enable to transfer the presented knowledge in this publication to the design procedure of rectangular shaped segments. A detailed adaption of the proposed model for more complex geometries and reinforcement layouts (e.g. for the longitudinal joint of a tunnel segment) is not part of this paper and will be done in a future research work. The respective behavior of the confinement types including the occurring transverse stresses is outlined in Fig. 2b and Fig. 2d. In areas adjacent to the contact surface both effects lead to transverse compressive stresses. Hence, the transverse reinforcement close to the contact surface can be completely assigned to the passive confinement. At a greater distance from the surface, however, tensile stresses occur due to the load distribution. These stresses are usually attributed to the transverse reinforcement. To enable a simplified analysis, the transverse stresses are captured by the corresponding mechanical approaches shown in

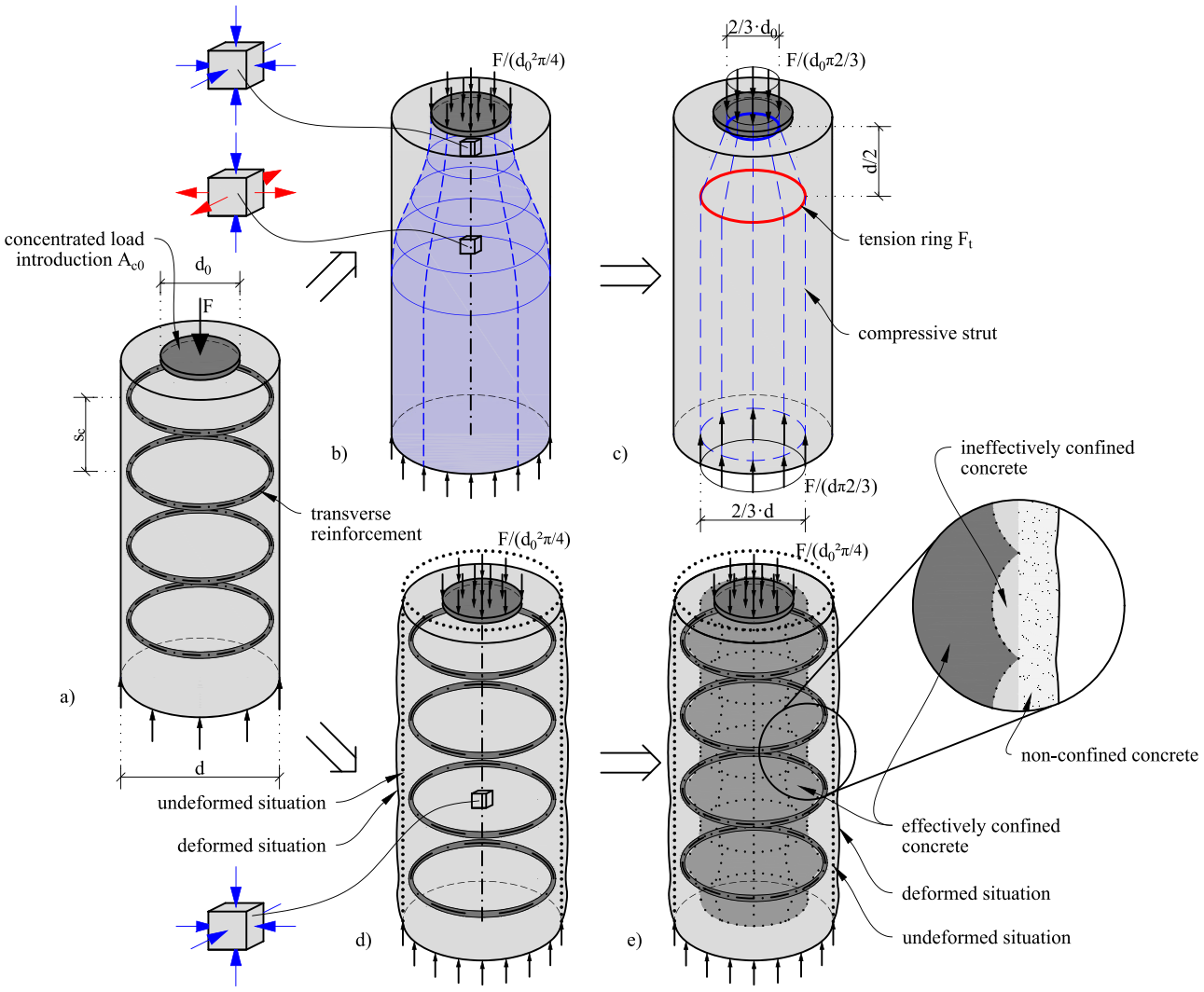

Fig. 2. Confinement in case of concentrated load introduction: (a) centrically loaded cylinder with transverse reinforcement, (b) mechanical behavior of load distribution, (c) model approach regarding the load distribution — strut-and-tie model, (d) mechanical behavior of passive confinement, (e) model approach of passive confinement — increase of the uniaxial compressive strength in the effectively confined concrete. (For interpretation of the references to color in this figure, the reader is referred to the web version of this article.).

Fig. 2c and Fig. 2e. The idea of the proposed model in Section 3 is to determine the triaxial compressive strength beneath the contact surface by combining the simplified approaches regarding geometric and passive confinement in a certain way. The two confinement effects themselves, are further discussed in Sections 2.1 and 2.2.

2.1. Geometric confinement:

In literature (e.g. [15]), a fundamental distinction is made between plane and spatial load distribution. With regard to the geometric confinement effect, a plane stress state occurs in the plane case (shown in Fig. 1b), while a triaxial stress state occurs in the spatial case (shown in Fig. 1a). In addition, triaxial stress states can also be found in plane load distribution if the transverse reinforcement is placed orthogonally to the direction of the load distribution. For this reason, the use of the terms plane geometric, plane passive, spatial geometric and spatial passive confinement is more precise than the mere distinction between plane and spatial load distribution.

While transverse compressive stresses (blue arrows orthogonal to the loading direction in Fig. 1a, 1b and 2b) are caused by the distribution of the compressive stress trajectories in the area immediately below the contact area, transverse tensile stresses (red arrows orthogonal to the loading direction in Fig. 1a, 1b and 2b) occur in the areas at a certain distance. In 1924, Mörsch [23] addressed the tensile stresses with a strut-and-tie model, which is still seen as state of the art in the current European design code [6]. A corresponding strut-and-tie model to the cylindrical test specimens investigated in this paper is given in Fig. 2c. The tensile force F_t, acting at a distance of approximately $0.5 \cdot d$, can be determined according to Eq. (1). Therein d_0 denotes the diameter of the contact surface and d the diameter of the concrete cylinder, which is equal to the diameter available for the load distribution.

$$F_t = \frac{F}{3\pi} \cdot \left(1 - \frac{d_0}{d}\right) \tag{1}$$

The model according the current EC2-draft [1] covering the geometric confinement effect is presented in Section 2.3.

2.2. Passive confinement:

While passive confinement in general is caused by transverse pressure that is activated by the impediment of lateral expansion, this paper only focuses on impediment caused by transverse reinforcement. For activating the transverse pressure, which is visualized with blue arrows orthogonal to the loading direction in Fig. 2d, a certain deformation is needed. In the unloaded state and early stage of loading mainly

transverse pressure caused by the unloaded concrete around the load application is generated. As the load increases and the tensile strength of concrete is exceeded, the impediment of the transverse strain is mainly caused by the transverse reinforcement. With increasing loading cracks appear in the non-confined concrete (which is the area between the center line of the reinforcement and the concrete surface), sometimes even leading to the spalling of the concrete. This, however does not interfere the confined concrete (which is separated into effectively and ineffectively confined concrete according Fig. 2e) to take on further loads resulting in even larger deformations. When reaching the peak load the compressive stresses in the effectively confined area can be far above the uniaxial concrete strength f_c and the transverse stresses generated by transverse reinforcement are limited with the yielding point of the steel reinforcement.

Passive confinement is also categorized into biaxial (shown in Fig. 1d) and triaxial stress states (shown in Fig. 1c). Hence, even in plane cases of load distribution, a triaxial stress state can be obtained through a spatial arrangement of adequate transverse reinforcement. This is the case if the reinforcement layout of Fig. 1c is implemented within the strip loaded concrete element shown in Fig. 1b. This situation can be found for example in the longitudinal joints of tunnel segments.

2.3. Existing models

In this section five models are presented and discussed, which can be applied to design a concentrated load introduction. They are used for a comparative calculation to validate the performance of the newly developed model which will be presented in Section 3. Therefore the nomenclature in this paper slightly defers from the original literature to be consistent with the terms and indices defined for the mechanical approach presented in Section 3. The two models according the EC2-draft [1] are presented in more detail, because they represent the state of the art of the future European design code.

2.3.1. Eurocode 2 - Section 8.6 (EC2 approach)

The EC2 approach [1] (square root equation) is dependent on the ratio between the area of the concrete available for the load distribution A_{c1} and the area of the contact surface A_{c0}. The increase factor for the uniaxial concrete strength $\sqrt{A_{c1}/A_{c0}}$ is based on empirical investigations according [9] and mainly covers the effect of geometric confinement. The load-bearing capacity is verified according to Eq. (2):

$$F_{cal.EC2} = A_{c0} \cdot f_c \cdot \sqrt{\frac{A_{c1}}{A_{c0}}} \leq v_{part} \cdot A_{c0} \cdot f_c \tag{2}$$

where v_{part} is a limiting factor restricted to $v_{part} = 3.0$ if no external tensile forces induce cracking in the direction parallel to the applied load. A requirement for using Eq. (2) is the limitation of the load distribution to the same distance in both transverse directions, which is fulfilled for the presented experiments in this paper. Regarding the application of Eq. (2) to tunnel segments, the limitation of the load distribution often is neglected based on experimental investigations from literature (e.g. [24,25]). The occurring splitting tensile forces have to be covered by transverse reinforcement, which can be determined according to Eq. (1).

2.3.2. Eurocode 2 - Section 8.14 ($EC2_{conf}$ approach)

The $EC2_{conf}$ approach [1] is presented in the first line of Eq. (3). For the prediction of the load-bearing capacity of the contact surface A_{c0}, the minimum of the confined concrete area A_{cc} and the contact surface A_{c0} is decisive (a definition of the concrete areas is outlined in Fig. 3). This specification is not discussed in the standard as it is originally developed for confined concrete elements without concentrated load introduction. To emphasize this consideration when applying $EC2_{conf}$ to load transfer zones, a min-function is used in the second line of Eq. (3). Furthermore the additive term to increase the compressive strength $\Delta f_{s.cc}$ is applied to the effective confined concrete area $A_{cc.e}$ which may not exceed the dimension of the contact surface A_{c0}. This geometrical restriction is also covered with a min-function in Eq. (3).

$$\begin{aligned} F_{cal.EC2conf} &= A_{cc} \cdot f_c + A_{cc.e} \cdot \Delta f_{s.cc} = \\ &= \min(A_{c0}; A_{cc}) \cdot f_c + \min(A_{c0}; A_{cc.e}) \cdot \Delta f_{s.cc} \end{aligned} \tag{3}$$

According to the EC2-draft [1] the effectiveness factors $k_{conf,b}$ and $k_{conf,s}$ lower the strength increase depending on the reinforcement layout. Instead of using a distributed strength over the whole cross section, the cross section can be separated into different areas as defined in Fig. 3. The effectively confined concrete area $A_{cc.e}$, can be further adapted for circular cross sections using the effectiveness factors $k_{conf,b} \cdot k_{conf,s}$ according to Eq. (4).

$$\begin{aligned} A_{cc.e} &= A_c \cdot k_{conf,b} \cdot k_{conf,s} = \\ &= \frac{\pi}{4} \cdot \left(d_c - \frac{s_c}{2}\right)^2 \end{aligned} \tag{4}$$

The compressive strength increase $\Delta f_{s.cc}$ due to a transverse compressive stress is to be calculated according to Eq. (5):

$$\Delta f_{s.cc} = \begin{cases} 4 \cdot \sigma_{cc} & \text{for } \sigma_{cc} \leq 0.6 f_c \\ 3.5 \cdot \sigma_{cc}^{\frac{3}{4}} \cdot f_c^{\frac{1}{4}} & \text{for } \sigma_{cc} > 0.6 f_c \end{cases} \tag{5}$$

with the transverse compressive stress σ_{cc} resulting from the transverse reinforcement is to be calculated according to Eq. (6). Therein A_s is defined as the cross-sectional area of a transverse reinforcement layer. For the material parameters and the geometries used for the test specimens in this publication the transverse stresses do not exceed $0.6 \cdot f_c$, which means only the first line of Eq. (5) is relevant in this paper.

$$\sigma_{cc} = \frac{A_s \cdot f_y}{s_c \cdot d_c} \tag{6}$$

The EC2-draft [1] provides a model for covering geometric confinement (EC2 approach) and another one for passive confinement ($EC2_{conf}$ approach), but does not give any advices how to combine these two approaches (EC2 and $EC2_{conf}$).

2.3.3. Schmidt-Thrö

The empirical design approach of Schmidt-Thrö [18] is based on a linear regression of an extensive experimental campaign on tunnel segments and is shown in Eq. (7). Therein the load distribution ratio A_{c1}/A_{c0} is used for determining the increase of the uniaxial concrete strength. It is the only model which was calibrated on experiments between two concrete elements instead of using a steel plate for applying a concentrated load.

$$F_{cal.Schmidt-Thrö} = A_{c0} \cdot f_{cm} \cdot \left(0.37 \cdot \frac{A_{c1}}{A_{c0}} + 0.76\right) \tag{7}$$

For covering the occurring tensile splitting forces, Schmidt-Thrö also recommends the determination of the splitting forces according to Eq. (1).

2.3.4. Wichers

The model developed by Wichers [15] is based on the model of Wurm and Daschner [19]. It distinguishes between a spatial and a plane load distribution. Applied to the presented cylindrical test specimens only the model for the spatial load distribution has to be considered. It belongs to the category of models which cover the geometric and passive confinement effects with empirically determined factors. The load-bearing capacity can be determined using Eq. (8).

$$F_{cal.Wichers} = A_{c0} \cdot f_{cm} \cdot \left(\sqrt{\frac{A_{c1}}{A_{c0}}} + 0.55 \cdot \rho\right) \tag{8}$$

The approach is originally limited for concrete elements with a maximum transverse reinforcement ratio of 1 %. For the calculations in this paper this limit is neglected to enable a comparison based on the experiments presented in Section 4.

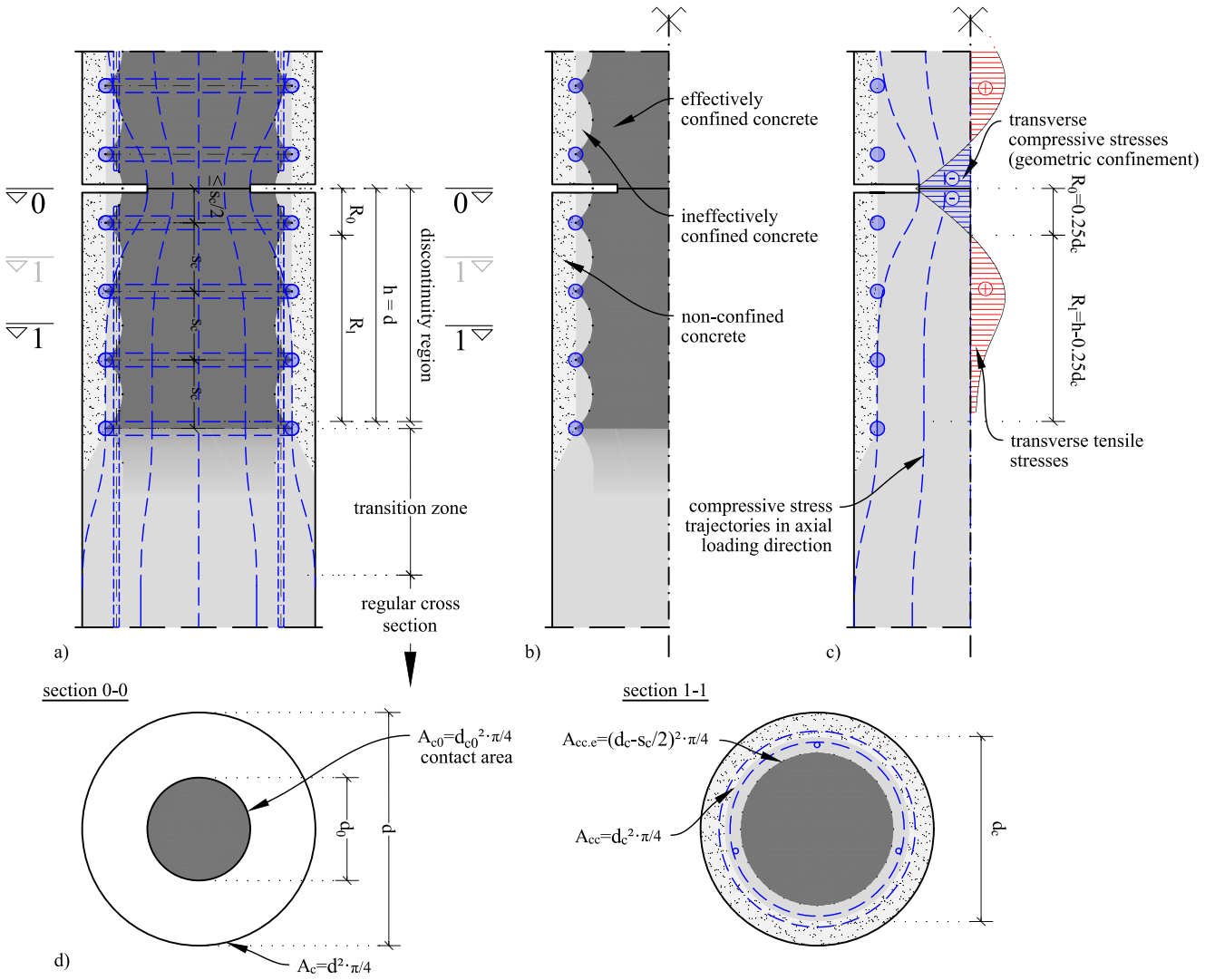

Fig. 3. Mechanical effects and their simplifications acting in a load transfer zone: (a) combination of all effects, (b) passive confinement caused by the transverse reinforcement, (c) load distribution which causes geometric confinement in R_0 and tensile stresses in R_1, (d) decisive cross sections.

2.3.5. Dual-cone (DC) stress field theory

In Markić et al. [4,26] it was shown, that the Dual-Cone (DC) stress field theory performs very well with the problem of concentrated load applications. This analytical approach based on the stress-field theory comes with the advantage of providing a solution without empirically determined factors. This model considers both, the geometric and passive confinement effect and it is explicitly allowed according the EC2-draft [1] to apply the stress field theory for situations of concentrated load introductions. Since the determination of the load-bearing capacity is an extensive iterative process, the analysis procedure of the DC-model has to be taken from Markić et al. [4].

3. Proposed geometric and passive confinement-model (GPC-model)

3.1. Assumptions and considerations

The goal of this paper is to predict the load-bearing capacity of load transfer zones with a mechanical approach, which is sufficiently simplified to be applied in a future design code. Therefore a model built on a mechanical basis and complemented by a semi-empirical component is presented as follows. The fundamental requirement for using the newly presented GPC-model (Geometric and Passive Confinement-model) is the presence of a triaxial stress state in the cross section of the contact area (section 0–0 in Fig. 3). This can be achieved by geometric confinement, passive confinement or a combination of both. Since there is an interaction between geometric and passive confinement, the different effective cross sections within and beyond the load transfer zone have to be considered for the design.

The discontinuity region is simplified into two regions (R_0 and R_1 which are shown in Fig. 3a for the bottom cylinder), based on the transverse stresses caused by the linear elastic load distribution. In region R_0 transverse compressive stresses (geometric confinement) occur beneath the contact area, where the trajectories are convex toward the centerline of the load transfer zone (shown in Fig. 3c). In region R_1 mainly transverse tensile stresses occur due to the load distribution. To simplify the complex stress situation in the discontinuity region two decisive cross sections (section 0–0 and 1–1) are defined for designing the load transfer zone shown in Fig. 3a and Fig. 3d. Section 0–0 is located in the contact area, which is the decisive section in region R_0. Section 1–1 is located at half the distance ($s_c/2$) between any two reinforcement layers located in region R_1. Since the cross section of the effectively confined concrete is variable along the height (shown in Fig. 3b), the decisive cross section for determining the load-bearing capacity is defined as $A_{cc.e}$ and located in section 1–1 (shown in Fig. 3d). The cross section of the confined concrete, which includes the effectively and ineffectively confined concrete, is constant along the entire discontinuity region and is defined as A_{cc}. Further the cross

section of the destroyed non-confined concrete does not contribute to the load-bearing capacity, when passive confinement is fully activated. For a proper application of the GPC-model the following considerations have to be taken into account in the design and analysis procedure:

- In the plane of the contact area the geometric and passive confinement effect can be considered to increase the bearing capacity. The height of the region, where geometric confinement may occur depends on the load concentration ratio and the type of load distribution (plane or spatial case). According to literature [27–29] the region, where transverse compressive stresses can occur in the linear elastic case, starts form the contact area and ends at 0.05 to 0.25 d_c. Therefore, a conservative assumption of $R_0 = 0.25\ d_c$ (shown in Fig. 3c) is made when applying the GPC-model.
- When the distance to the contact area increases, tensile forces have to be taken into account. These forces, which can be determined using the well known strut-and-tie model according to Mörsch [23], reduce the beneficial effect of the passive confinement and have to be additionally considered when assessing the load-bearing capacity in section 1–1. In this paper the strut-and-tie model according Fig. 2c was generalized to be applied to rotationally symmetric cylinders and their individual reinforcement layout. For the simplification of the GPC-model the determined tensile force is then assigned equally to the accountable reinforcement layers n_{sp} in region R_1. Considering the structural requirements for practical applications e.g. tunnel segments (concrete cover and minimum distance between two reinforcement layers) usually all reinforcement layers exclusive the first one fulfill the criteria defined in Section 3.2 to assign tensile forces.
- When surpassing the discontinuity region, the load-bearing capacity of the regular cross section (shown in Fig. 3) can be determined without reducing the cross section. In the transition zone between the last reinforcement layer, which provides confinement, and the regular cross section the occurring splitting stresses are usually covered by the tensile strength of the concrete. In the case of a relatively large area of non-confined concrete or a very high transverse reinforcement ratio (both lead to high splitting stresses) the transition zone needs to be checked in detail. Since the publication only focuses on the load transfer zone, the transition zone is not discussed in detail.

The GPC-model was developed for reinforced concrete structures where the formation of a triaxial stress state can be ensured. Unreinforced concrete elements or situations, where the reinforcement only ensures a plane stress state are not covered by the GPC-model.

3.2. Analysis procedure

Based on the two failure regions (R_0 and R_1) mentioned above, it can be stated that the minimum load-bearing capacity of section 0–0 and 1–1 (shown in Fig. 3a and Fig. 3d) is decisive for designing a load transfer zone. The analysis procedure is presented in the following sections.

Limit state of the contact area A_{c0} (section 0–0)

The load-bearing capacity of a geometrically and passively confined contact surface according to Eq. (9) is divided into three components. The first component F_{cm} refers to the uniaxial concrete compressive strength f_{cm}. The second component ΔF_c can be defined as an increasing term, which considers the geometric confinement effect. The third component $\Delta F_{s.cc}$ (where $s.cc$ stands for steel confined concrete) considers the increase due to the transverse reinforcement (passive confinement). Eq. (9) is based on mechanical considerations of previous publications [13,15–17,26], where it was already proven, that the geometrical and passive confinement both influence the load-bearing capacity of the contact region (section 0–0).

$$F_{cal.GPC0} = F_{cm} + \Delta F_c + \Delta F_{s.cc} = \\ = \underbrace{f_{cm} \cdot A_{c0}}_{F_{cm}} + \underbrace{\Delta f_c \cdot A_{c0}}_{\Delta F_c} + \underbrace{\Delta f_{s.cc} \cdot \min(A_{c0}; A_{cc.e})}_{\Delta F_{s.cc}} \tag{9}$$

The load-bearing capacity component ΔF_c is caused by load concentration in the contact area. This geometrical situation leads to a redirection of the stress trajectories in the confined concrete area (shown in Fig. 3c) and is defined as geometric confinement. The empirical function for capturing the concrete strength increase caused by the load distribution Δf_c is proposed in Eq. (10), which is based on the fundamental experiments of Spieth [9,13]. Therein the innovation, in comparison to existing approaches, is the consideration of A_{cc} instead of A_c for the determination of the load-bearing increase caused by the application to a confined concrete area. The idea to consider only the confined concrete core for determining the geometric confinement effect for a combined approach is based on the fact, that in passively confined elements the non-confined concrete should not be considered for the load-bearing capacity, which is suggested in literature [7,8,12,30].

$$\Delta f_c = f_{cm} \cdot \left(\left(\frac{A_{cc}}{A_{c0}} \right)^{\frac{1}{2}} - 1 \right) \geq 0 \tag{10}$$

The load-bearing capacity component $\Delta F_{s.cc}$ is caused by the confinement effect due to the transverse reinforcement and is based on a mechanical approach. It is assumed, that the transverse reinforcement causes an effectively confined concrete core (shown in Fig. 3b) with a triaxial stress state. The increase of the compressive strength $\Delta f_{s.cc}$ in the contact area can be calculated according to Eq. (5). For the determination of the transverse compressive stress σ_{cc} it can be assumed, that the transverse reinforcement reaches the yield stress according to Eq. (6).

Limit state of the decisive section in region R_1 (section 1–1)

Along the region R_1 the weakest section is found halfway between two transverse reinforcement layers with the load-bearing capacity determined according to Eq. (11).

$$F_{cal.GPC1} = F_{cm} + \Delta F_{s.cc} = \underbrace{f_{cm} \cdot A_{cc}}_{F_{cm}} + \underbrace{\Delta f_{s.cc} \cdot A_{cc.e}}_{\Delta F_{s.cc}} \tag{11}$$

The positive effects of the passive confinement are calculated using the previously presented mechanical model according to Eq. (5). The determination of the transverse compressive stress σ_{cc}, which was shown in Eq. (6), has to be adapted in order to consider the unfavorable tensile force F_t in the tensile ring according to Eq. (12). A visualization of assigning the tensile forces to the accountable reinforcement layers is shown in Fig. 4a.

$$\sigma_{cc} = \frac{A_s \cdot f_y - 2F_t/n_{sp}}{s_c \cdot d_c} \tag{12}$$

with:

A_s Cross-sectional area of a transverse reinforcement layer (for a cylindrical hoop $A_s = 2(\varnothing^2 \pi/4)$)

The tensile force F_t is determined by the generalized strut-and-tie model according Eq. (13), which is shown in Fig. 4b. In comparison to Eq. (1), the generalized model is applied to the load distribution in the confined concrete area. The center of gravity of the accountable reinforcement layers n_{sp} (colored in red in Fig. 4a) defines the location of F_t, which can be seen in Fig. 4b.

$$F_t = \frac{F}{6\pi} \cdot \left(\frac{d_c - d_0}{x_{sp}} \right) \tag{13}$$

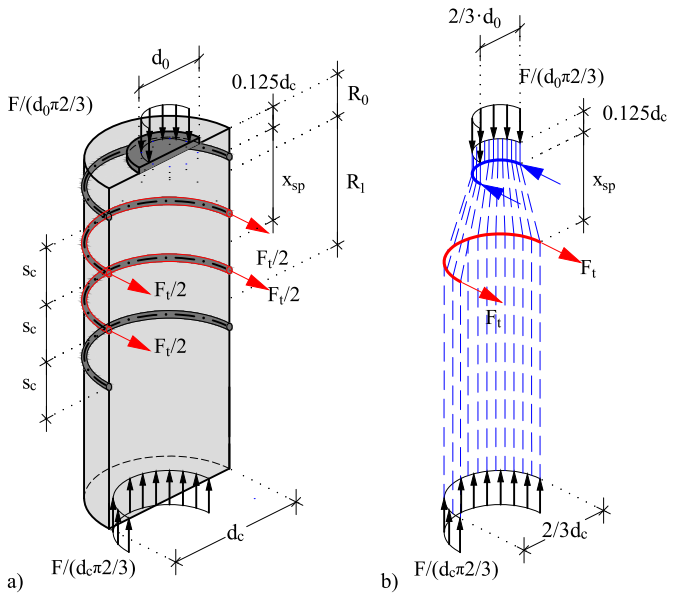

Fig. 4. (a) Assignment of F_t to the accountable reinforcement layers in region R_1, (b) generalized strut-and-tie model for determining F_t. (For interpretation of the references to color in this figure, the reader is referred to the web version of this article.).

with:

F Axial load applied on the load transfer zone limited by $F_{cal.GPC0}$

x_{sp} Distance between the compression ring and the resulting tensile force depending on the center of gravity of the accountable reinforcement layers (shown in Fig. 4b)

To follow the linear elastic stress distribution only a certain number of reinforcement layers n_{sp} (determined by Eq. (14)) are allowed to be considered for assigning the tensile force.

$$n_{sp} = \left(n_0 + n_1\right) - \max(1; n_0) \tag{14}$$

with:

n_0 number of reinforcement layers located in R_0

n_1 number of reinforcement layers located in R_1

In Fig. 4a the tensile force is assigned to the second and third reinforcement layer (colored in red), which reduces the passive confinement effect of these reinforcement layers. Based on this simplification the load-bearing capacity of R_1 can be determined by the decisive load-bearing capacity of section 1–1. This procedure only works for a constant spacing s_c between the reinforcement layers placed in the discontinuity region.

Transition zone and regular cross section next to the load transfer zone

The load-bearing capacity of the transition zone and the regular cross section next to the discontinuity region can be determined considering the full cross sectional area A_c. The low tensile stresses in the transition zone are usually covered by the tensile strength of the concrete. Special attention has to be paid to the transition zone in the case of a relatively large area of non-confined concrete or a very high transverse confinement in the load transfer zone.

4. Experimental investigations

In order to achieve a better understanding of the load-bearing mechanisms and their interaction, the conducted experiments focus on fundamental investigations. Therefore relatively small specimens with simple geometric conditions in comparison to tunnel segments are assessed with the goal of transferring the gained knowledge to the design procedure of larger segments. Since the proposed mechanical model relies on mechanical principals supplemented by a well known empirical term, it is possible to adapt the model to other geometric situations.

4.1. Testing procedure

The experimental campaign was designed to validate the new mechanical approach for predicting the load-bearing capacity of geometrically and passively confined load transfer zones. In two Series (1 and 2) 13 different specimen types (shown in Fig. 5) and a total amount of 26 tests were performed to investigate the load-bearing capacity of load transfer zones under centric loading. Each type of test was performed twice in order to validate the respective results, with the nomenclature of V1 and V2 for the first and second test which was executed. Every test consisted of two identical concrete specimens, which were pressed against each other until the peak load was reached and a significant load drop could be observed in the post-failure behavior.

The GPC-model was developed based on mechanical considerations from literature and verified using the presented experimental campaign. The following parameters regarding the geometry and the reinforcement layout are investigated in detail:

- The transverse reinforcement ratio $\rho = A_s/(s_c \cdot d_c)$ in the area of the load transfer zone was chosen in regard to practical relevance in a range between 0 % and 2.57 %.
- The ratio of the area available for load distribution and the contact surface A_{cc}/A_{c0} was chosen between 1.0 and 3.3. Higher load concentrations, which are less relevant for practical applications, can also be assessed by the model and are investigated in Section 5.4.
- The first transverse reinforcement element was placed not further than $0.5 \cdot s_c$ from the contact surface to guarantee a passive confinement effect of the reinforcement for the limit state of the contact surface (section 0–0).

The range of the investigated parameters is further extended by a validation with tests from literature presented in Section 5.4. A final proposal concerning the application limits and the design recommendations for load transfer zones is given in Section 5.6.

4.2. Test specimens

The experimental campaign (shown in Fig. 5) consists of two series; Series 1 focuses on the variation of the reinforcement layout and Series 2 investigates variable load concentration ratios and different materials used for introducing the concentrated load. All specimens were produced with a height H of 300 mm and a diameter d of 150 mm, which was reduced to d_0 (according to Table 2), apart for reference specimens A1 and H2, at the ends of the specimens over a height of 3 mm. The diameter of the used reinforcement bars was varied from ⌀ 4 mm for the mounting bars to ⌀10 mm for the specimens with the highest reinforcement ratio. Larger reinforcement diameters were not used as the predefined dimensions of the specimens required a small bending radius. The ends of the reinforcement hoops were butt welded to eliminate inaccuracies due to the overlap of conventionally manufactured hoops. Therefore the spacing between the transverse reinforcement layers s_c could be manufactured with a tolerance of ±1 mm.

For the specimen types B1 to G1 of Series 1 the diameter d_0 was reduced to 101 mm leading to a load concentration ratio A_{cc}/A_{c0} for C1 to G1 of 1.81 and 2.21 for B1 (unreinforced specimen with A_{cc} assumed as A_c). For the design of the test specimens, the load concentration ratio

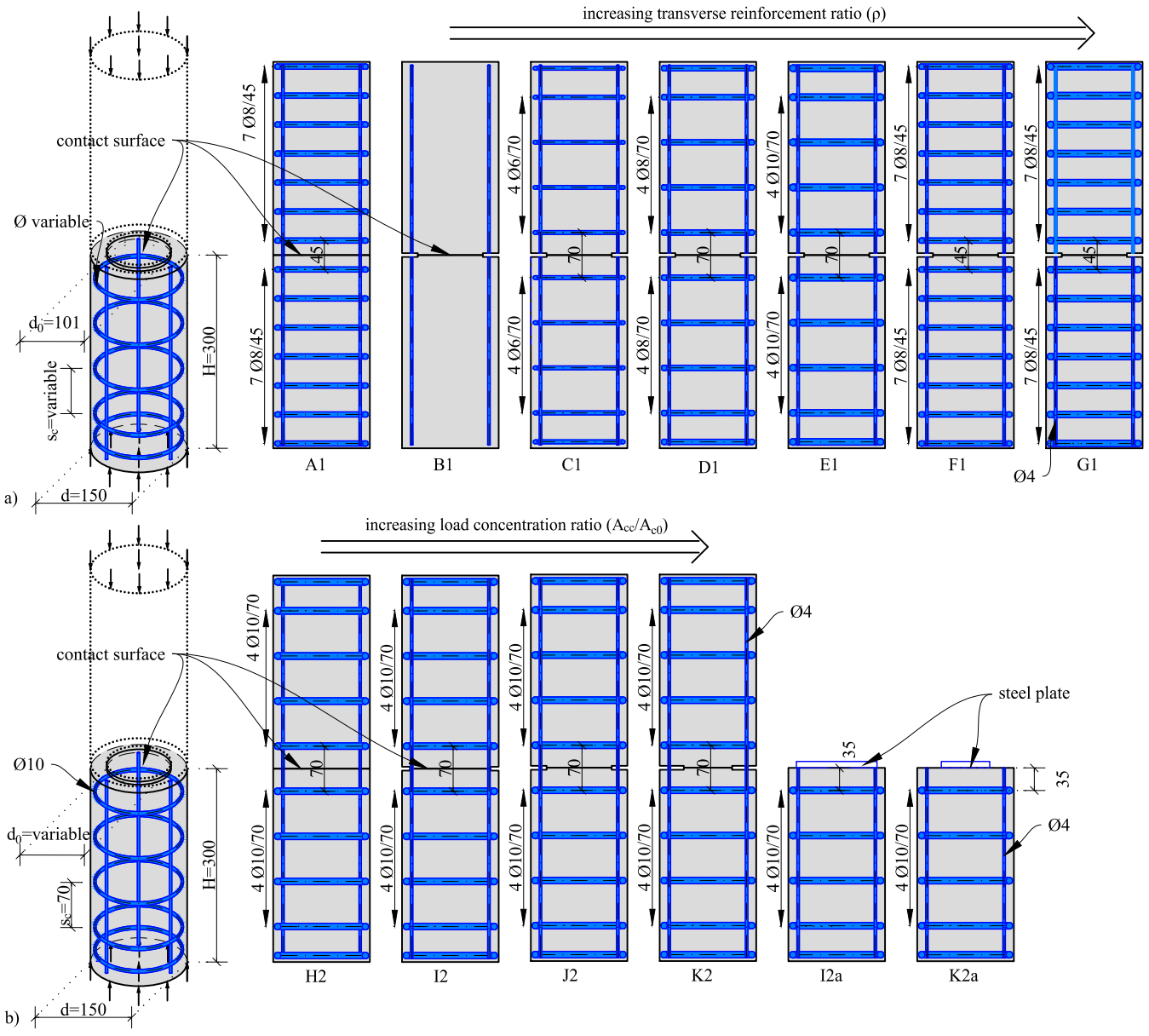

Fig. 5. Geometry and reinforcement layout of the test specimens with all units in [mm]; (a) Series 1; (b) Series 2.

was based on typical values used for tunnel segments. The dimensions of the test specimens were kept constant to investigate the influence of the reinforcement layout. This was accomplished by varying the bar diameter ⌀ and the spacing s_c between the hoops in order to achieve a continuous increase of the reinforcement ratio ρ from 0 % in B1 to 2.57 % in G1. Since the distance between the hoops across the contact surface is decisive for the failure of the load transfer zone, special attention was paid to the manufacturing accuracy during the production of the reinforcement cages. All test specimens were uniformly reinforced over the entire height (shown in Fig. 5), to prevent failure adjacent to the discontinuity region. Furthermore, the transverse reinforcement was designed to cover the occurring tensile forces according to the strut-and-tie model to prevent failure at the plane of section 1–1.

The diameter referred to the center line of the hoops amounted to 136 mm and therefore resulted in varying concrete covers (from 2 mm to 4 mm) for the different bar diameters. The thickness of the non-confined concrete was kept to a minimum in order to monitor the behavior of the confined concrete core when reaching the failure load.

For the specimen types H2 to K2 of Series 2 the reinforcement layout was kept constant with a geometrical reinforcement ratio of ρ = 1.65 %, corresponding to a typical amount of reinforcement in practical applications. The load concentration, quantified by the ratio A_{cc}/A_{c0}, was increased from 1.0 to 3.3 in order to investigate the influence of the geometric confinement under these conditions. For the specimen types I2a and K2a a high-strength steel plate was used for load introduction instead of the concrete–concrete (c–c) load transmission, allowing for a direct investigation of the influence of the load application types. These two types (c–c and st–c) were chosen as they represent, on the one hand, the most realistic setup and, on the other hand, the most convenient load introduction system frequently used in literature [9,16,17,19–21].

The material properties of all specimen components are summarized in Table 1. Normal concrete with a mean compressive strength between 48.0 N/mm^2 and 55.6 N/mm^2 and a maximum aggregate size of D_{max} = 16 mm was used. The compressive strength was determined by testing multiple samples according to ONR 23303 [31]. Instead of storing the specimens in a water bath the cylinders were exposed to the same weathering conditions as the test specimens. To minimize the effect of concrete aging all tests were performed at ages above 28 days. The

Table 1
Material properties.

Material	f_{cm} [N/mm²]	$f_{cm,cube}$ [N/mm²]	f_{ctm} [N/mm²]	f_{ym} [N/mm²]	E_{cm} [N/mm²]
Concrete Series 1	48.0	61.8	3.1	–	29 395
Concrete Series 2, Batch 1	55.6	–	3.2[a]	–	29 979
Concrete Series 2, Batch 2	52.8[b]	66.0	3.2[a]	–	–
Reinforcement steel B550B	–	–	–	580[c]	200000[a]
High strength steel 1.2312	–	–	–	≈1100[d]	210000[d]

[a] Determined according to EN 1992-1-1 [1].
[b] Determined with $0.8 \cdot f_{cm,cube}$.
[c] Rounded value based on 9 samples with 3 different diameters with f_{ym} = 581.5 N/mm² (COV = 1 %).
[d] According to the technical data sheet [32].

steel plates, which were used for load introduction, were made of high-strength steel with a strength twenty times higher than the concrete strength of the test specimens.

4.3. Test setup

All tests were carried out in a vertical testing rig at the laboratory of the Institute of Structural Engineering. The compressive load was applied displacement-controlled with a speed between 0.1 mm/min and 0.2 mm/min. The specimens were tested under uniaxial pressure with installation tolerances of ±1 mm. Four linear variable differential transformers (LVDTs) were used to monitor the displacements in direction of the load introduction (shown in Fig. 6). To prevent an early failure of the test specimens due to imperfections of the concrete interface, two additional confining steel elements were installed next to the load introducing steel plates (for I2a and K2a only one bottom element was used). In order to better assess the failure process and crack development, digital image correlation (DIC) measurements (Aramis by Gom GmbH) were applied to one side of the test specimens.

5. Results and discussion

5.1. Load-bearing behavior

In all executed tests, a progressive load drop occurred after the peak load was reached. The load–strain curves of all experiments can be found in Appendix A, where Series 1 is shwon in Fig. A.1 and Series 2 in Fig. A.2 . The abrupt load drop post failure in some of the tests can be explained by a sudden failure of the welding points of the first or second stirrup next to the contact surface (e.g. Fig. A.1a and Fig. A.1c). Experiments with very extensive post-failure behavior (without failure of the welding point) were stopped when a deformation of 1.3 to 2.0 times ε_u was reached.

When reaching the peak load, the reference specimens with exclusively passive confinement (A1 and H2) showed longitudinal cracks in the area between the stirrups and circumferential cracks at the level of the stirrup reinforcement. In the post-failure behavior, the parabolic fracture pattern, known from tests of passively confined columns, developed. As the failure planes of the specimens A1-V1, A1-V2, and H2-V2 were located at distances of 90 mm, 135 mm and 70 mm from the contact area, a significant influence of the contact area on the ultimate load under centric compressive loading can be excluded.

The unreinforced test specimens B1 showed no noticeable cracks when the peak load was reached. A brittle failure occurred, as can be deduced from the load–strain curves in Fig. A.1b, which can be assigned to a splitting tensile failure in the discontinuity region (section 1–1).

Once the peak load was reached, longitudinal cracks were monitored in the discontinuity areas of all reinforced test specimens. With a growing transverse reinforcement ratio, the number of longitudinal cracks increased as well. This observation confirms the theoretical assumption in the GPC-model that the non-confined concrete area ($A_c - A_{cc}$) is no longer relevant for predicting the load-bearing capacity.

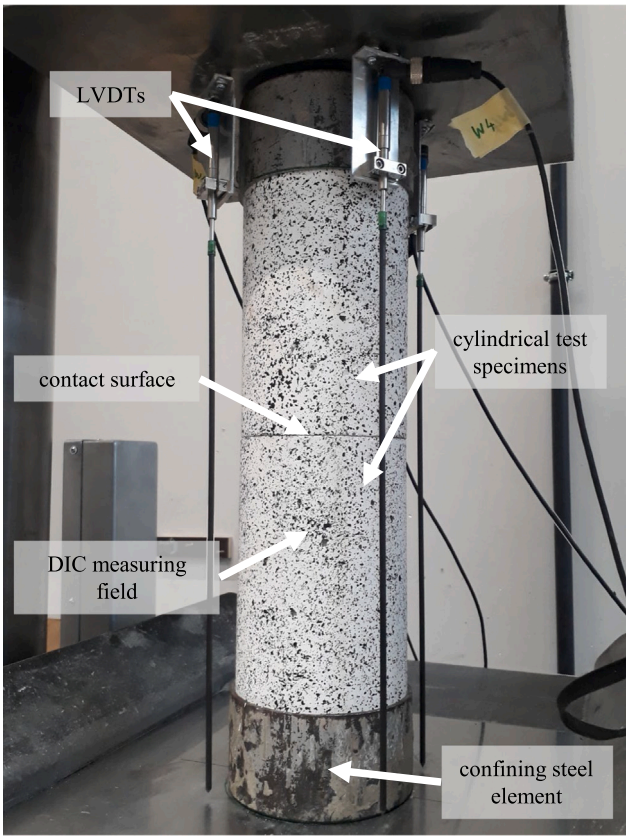

Fig. 6. Test setup at TU Wien.

For the test specimens with geometric and passive confinement (C1 to G1 and I2 to K2), the failure can be assigned to the area of the contact surface (section 0–0). The position of the failure plane was detected by visual inspection of all surfaces, fractures and plastic deformations of the test specimens after the test was finished. This specific failure is difficult to distinguish from a splitting tensile failure when analyzing the crack pattern at the moment of reaching the peak load, as can be seen using the DIC measurements for test J2-V1 in Fig. 7. In the post-peak period, however, further plastic deformations can be monitored that clearly identify the occurring failure mechanism. With the exception of the unreinforced test specimens, an extensive destruction of the concrete microstructure close to the contact area and a failure of the first reinforcement layer adjacent to the contact area (shown in Fig. 7b) was observed in all specimens.

The increase in the transverse reinforcement ratio ρ leads to higher stresses in the contact joint and a significant increase in the longitudinal ultimate strain ε_u, as clearly shown in Table 2 for all test results. The increase of the load distribution ratio also leads to higher stresses in the contact area but has no significant influence on the longitudinal

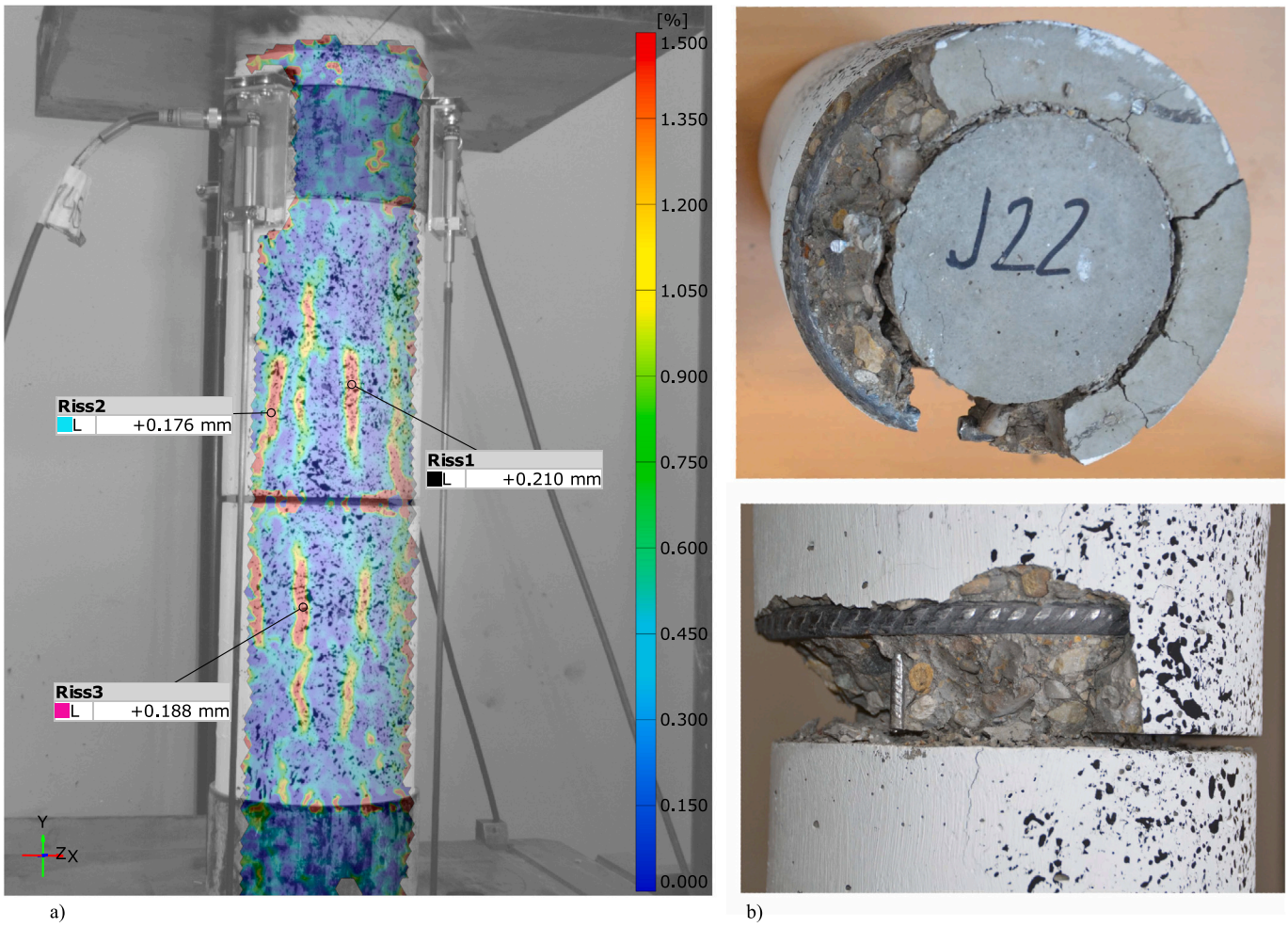

Fig. 7. Specimen J2-V1: (a) Crack pattern at peak load illustrated by the major strain in y-direction, (b) failure plane after testing.

ultimate strain ε_u. It has to be stated, that higher stresses due to higher geometric confinement do not lead to higher absolute peak loads, since an increase of the load distribution ratio results in the direct reduction of the contact area A_{c0}.

5.2. Model verification

The satisfactory performance of the GPC-model in predicting the load-bearing capacity is visualized in Fig. 8 where the experimental peak loads F_{exp} are compared to the top of the stacked gray colored bars ($F_{cal.GPC0} = F_{cm} + \Delta F_c + \Delta F_{s.cc}$). The results of Series 1 show that the passive confinement effect has a significant impact on the load-bearing capacity of load transfer zones. By looking at C1 to G1 (varying reinforcement ratio ρ) a continuous increase of the peak load can be seen, which can be covered by the geometric confinement component $\Delta F_{s.cc}$.

The experiments H2 to K2 (constant reinforcement ratio was kept and varying ratio of A_{cc}/A_{c0} does influence the bearing capacity of all three components (F_{cm}, ΔF_c and $\Delta F_{s.cc}$). Due to the separated consideration of the load-bearing components, this trend can be covered as well by the GPC-model.

The predicted total load-bearing capacity according to the presented GPC-Model agrees very well with the experimental data. In the next step the accuracy of the geometric and passive confinement shares were investigated. Therefore the individual load-bearing components were isolated based on the experimental dataset and compared with the presented mechanical approaches according to the following procedure:

1. The individual components of the load-bearing capacity are normalized in Eq. (15) by dividing Eq. (9) by the uniaxial concrete strength f_{cm}.
2. The components have to be related to the section of the contact area A_{c0} which turns Eq. (9) into Eq. (15). This expression allows a direct comparison of the experimental results with different concrete compressive strengths, contact areas and reinforcement ratios.

$$\frac{\sigma_{c0}}{f_{cm}} = \frac{1}{f_{cm}} \cdot \left(\underbrace{\frac{F_{cm}}{A_{c0}}}_{f_{cm}} + \underbrace{\frac{\Delta F_c}{A_{c0}}}_{\Delta f_c} + \underbrace{\frac{\Delta F_{s.cc}}{A_{c0}}}_{\Delta \sigma_{s.cc}} \right) = \tag{15}$$

3.1 The normalized increase factor of the geometric confinement ($\sigma_{c0}/f_{cm} - \Delta\sigma_{s.cc}/f_{cm}$) can be separated according to Eq. (16) by transforming Eq. (15) and replacing ΔF_c by the related expression in Eq. (9) and (10). The expression $\Delta\sigma_{s.cc}$ stands for the compressive strength increase due to steel confined concrete uniformly distributed over the contact surface A_{c0}.

$$\frac{\sigma_{c0}}{f_{cm}} - \frac{\Delta\sigma_{s.cc}}{f_{cm}} = \left(\frac{A_{cc}}{A_{c0}}\right)^{\frac{1}{2}} \tag{16}$$

3.2 The normalized increase factor of passive confinement ($\sigma_{c0}/f_{cm} - \Delta f_c/f_{cm}$) in Eq. (17) can be separated with similar steps of derivation as those used for Eq. (16). Starting

Table 2
Properties and experimental data of Series 1 and Series 2.

Test	f_{cm}	d_0	s_c	ρ	ω	A_{cc}/A_{c0}	F_{exp}	ε_u	σ_{c0}/f_{cm}
–	[N/mm²]	[mm]	[mm]	[–]	[–]	[–]	[kN]	[–]	[–]
A1-V1	48.0	150	45	0.0164	0.198	1.00[a]	1154	0.00772	1.36
A1-V2	48.0	150	45	0.0164	0.198	1.00[a]	1151	0.00829	1.36
B1-V1	48.0	101	0	0.0	0.0	2.21[a]	529	0.00176	1.38
B1-V2	48.0	101	0	0.0	0.0	2.21[a]	526	0.00179	1.37
C1-V1	48.0	101	70	0.0059	0.072	1.81	646	0.00291	1.68
C1-V2	48.0	101	70	0.0059	0.072	1.81	684	0.00296	1.78
D1-V1	48.0	101	70	0.0106	0.128	1.81	769	0.00431	2.00
D1-V2	48.0	101	70	0.0106	0.128	1.81	745	0.00463	1.94
E1-V1	48.0	101	70	0.0165	0.199	1.81	832	0.00488	2.16
E1-V2	48.0	101	70	0.0165	0.199	1.81	851	0.00568	2.21
F1-V1	48.0	101	45	0.0164	0.198	1.81	867	0.00532	2.25
F1-V2	48.0	101	45	0.0164	0.198	1.81	902	0.00671	2.35
G1-V1	48.0	101	45	0.0257	0.310	1.81	1022	0.00816	2.66
G1-V2	48.0	101	45	0.0257	0.310	1.81	1082	0.00990	2.81
H2-V1	52.8	150	70	0.0165	0.181	1.00[a]	1033	0.00520	1.11
H2-V2	52.8	150	70	0.0165	0.181	1.00[a]	1014	0.00543	1.09
I2-V1	52.8	125	70	0.0165	0.181	1.18	980	0.00555	1.51
I2-V2	52.8	125	70	0.0165	0.181	1.18	985	0.00571	1.52
J2-V1	52.8	101	70	0.0165	0.181	1.81	868	0.00526	2.05
J2-V2	52.8	101	70	0.0165	0.181	1.81	807	0.00473	1.91
K2-V1	55.6	75	70	0.0165	0.172	3.29	614	0.00488	2.50
K2-V2	55.6	75	70	0.0165	0.172	3.29	608	0.00461	2.48
I2a-V1	52.8	125	70	0.0165	0.181	1.18	1052	0.00634	1.62
I2a-V2	52.8	125	70	0.0165	0.181	1.18	1001	0.00578	1.54
K2a-V1	55.6	75	70	0.0165	0.172	3.29	665	0.00532	2.71
K2a-V2	55.6	75	70	0.0165	0.172	3.29	636	0.00601	2.59

[a] Determined with A_c/A_{c0}.

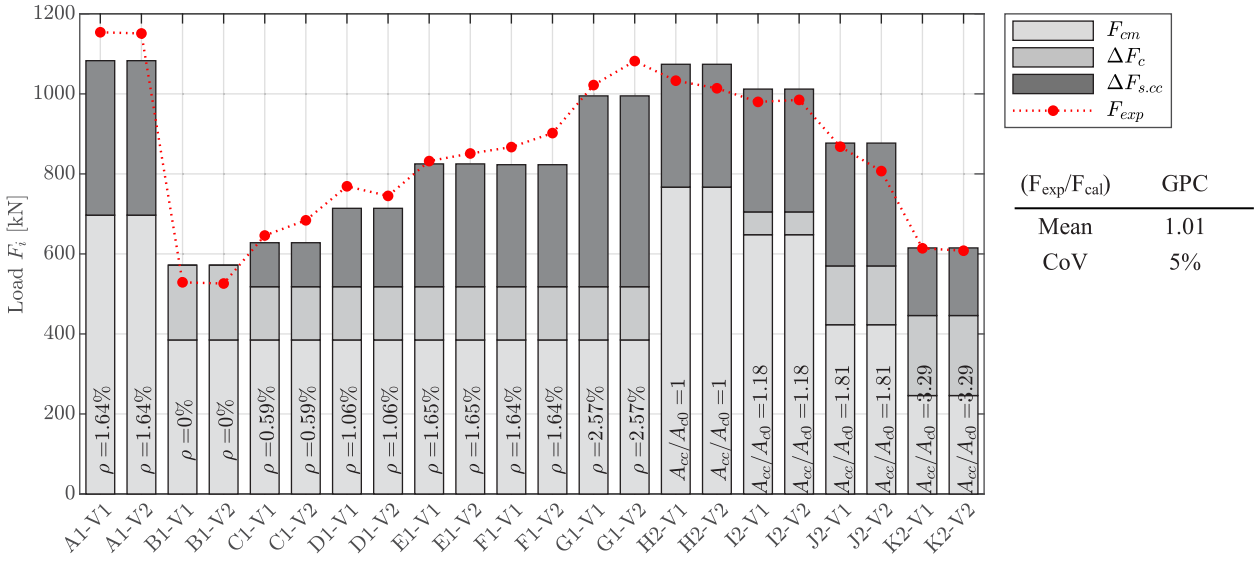

(F_{exp}/F_{cal})	GPC
Mean	1.01
CoV	5%

Fig. 8. Experimental and calculated load-bearing capacities of Series 1 and Series 2.

from Eq. (15) the term $\Delta F_{s.cc}$ has to be replaced by the related expression in Eq. (5) and (9). For the conducted experiments σ_{cc} is always smaller than $0.6 f_{cm}$ explaining why $\Delta f_{s.cc}$ was considered with $4 \cdot \sigma_{cc}$ in Eq. (5). Since the decisive cross section for applying the passive confinement always equals A_{c0} (except I2) the last part of (17) can be simplified to 1. In case of I2 with $A_{cc.e} < A_{c0}$, the normalized increase factor regarding passive confinement ($\sigma_{c0}/f_{cm} - \Delta f_c/f_{cm}$) cannot be compared to $\Delta f_{s.cc}/f_{cm}$ directly. Therefore specimen type I2 was neglected for this simplification

$$\frac{\sigma_{c0}}{f_{cm}} - \frac{\Delta f_c}{f_{cm}} = \\ = 1 + 4 \cdot \underbrace{\rho \cdot \frac{f_{ym}}{f_{cm}}}_{\omega} \cdot \underbrace{\min(A_{c0}; A_{cc.e}) \cdot \frac{1}{A_{c0}}}_{\approx 1} = \\ = 1 + 4 \cdot \omega \tag{17}$$

4. As a result the left side of Eqs. (16) and (17) are plotted in Fig. 9 using the experimentally determined stresses in the contact area ($\sigma_{c0} = \sigma_{c0.exp}$) and the material properties according to

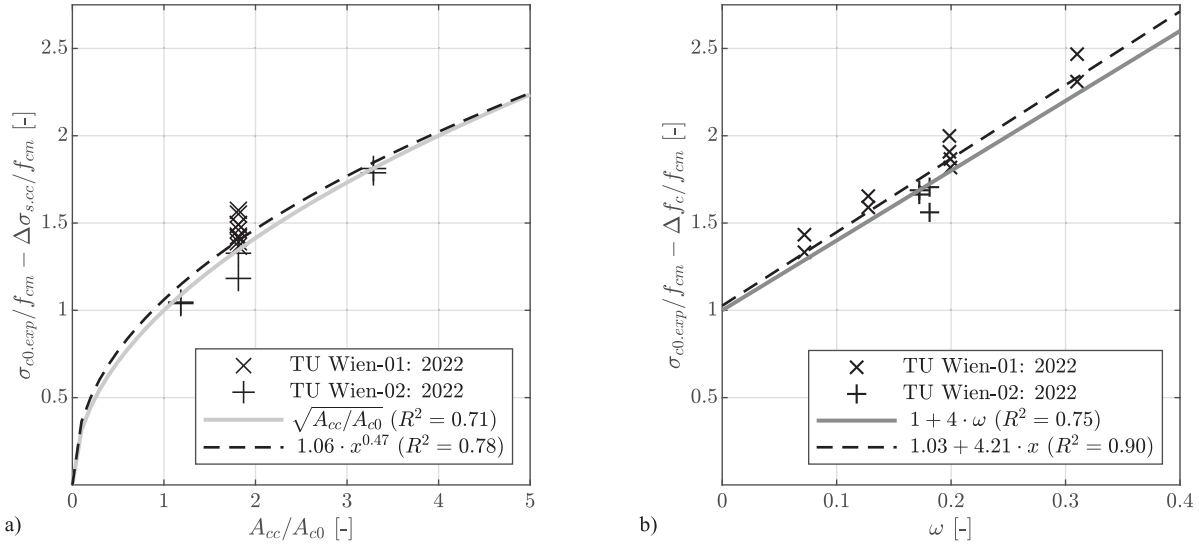

Fig. 9. Stress increase in the contact surface due to (a) geometric confinement as a function of the ratio between A_{cc}/A_{c0}, (b) passive confinement as a function of the transverse mechanical reinforcement ratio ω.

Table 1 showing a good agreement with the theoretical function on the right side of the equations. It must be mentioned that only experiments with a reduced contact surface and transverse reinforcement were considered.

In Fig. 9a the selected experimental dataset is plotted as a function of the ratio between A_{cc}/A_{c0}. The dashed line is a single term power fit of the experimental results. The solid line represents the increase factor of the geometric confinement, according to the GPC-model which corresponds well with the experimental dataset. The performance of the passive confinement approach is described by a 1st order polynomial fit, which is plotted as a function of ω in Fig. 9b. By comparing the polynomial fit (dashed line) with the chosen mechanical approach to describe the passive confinement effect (gray line) the good agreement can be confirmed.

Based on the verification shown in Fig. 8 and Fig. 9 it can be stated, that the GPC-model and its components provide quite accurate results to describe the load increase due to geometric and passive confinement.

5.3. Comparison with existing models

In the following section the GPC-model (Geometric and Passive Confinement-model) is compared to five models from literature, which were presented in Section 2.3 for predicting the bearing capacity of concentrated load applications.

In Fig. 10 and Fig. 11 the ratios of experimental and predicted load-bearing capacities are plotted using the previously discussed models, including the newly presented GPC-model. Out of 26 tests done at TU Wien 16 tests addressing load transfer zones with both transverse reinforcement and load concentration were used for the comparison. Specimen type A1, B1, H2, I2a and K2a were excluded because they do not meet the application requirements of some of the previously presented models. To avoid brittle failure all the design approaches need or recommend a minimum of transverse reinforcement. For determining the calculated load-bearing capacities in Fig. 10 and Fig. 11, the mounting bars ⌀ 4 mm, which are orientated parallel to the loading direction (shown in Fig. 5), have been neglected due to their relatively small load-bearing capacity.

The GPC and DC approaches provide the best predictions applied to the presented experimental campaign with a mean value of F_{exp}/F_{cal} = 1.02 and 0.98, respectively. Both the variation of the load concentration (shown in Fig. 10a and 10b) and the transverse reinforcement ratio (shown in Fig. 11a and 11b) are covered by the two models. In comparison to the DC-model the GPC-model can also be applied to specimens with pure passive confinement (A1 and H2 which was done in Fig. 8) and the analysis procedure in general is more user-friendly.

The approach of Wichers [15] significantly overestimates the ultimate loads with a mean value of F_{exp}/F_{cal} = 0.89. The model was developed for concrete elements with a transverse reinforcement ratio ρ of less than 1 %. Since only two of the 16 investigated tests had a transverse reinforcement ratio of less than 1 %, this might be an explanation for the deviation of the model. Fig. 10c shows, that the purely empirical factors, which are used in Wichers [15] to represent the geometric and passive confinement effects are inaccurate when it comes to small load distribution ratios A_{cc}/A_{c0}.

The approaches of Schmidt-Thrö and EC2 [1], which only consider the geometric confinement effect, are not able to cover situations with an increasing reinforcement ratio (shown in Fig. 11d and 11f). This leads to experimentally determined capacities up to 1.8 and 1.9 times higher than the prediction which can be seen in Fig. 10d, 10f, Fig. 11d and 11f. This problem can be solved with the GPC-model, which can be seen in Fig. 11a where the model yields accurate results along the whole spectrum of practically relevant reinforcement ratios.

The $EC2_{conf}$ approach [1] considers the passive confinement effect but does not predict accurately when the ratio A_{cc}/A_{c0} is increased. This trend can be seen by looking at the inclination of the 1st order polynomial fit in Fig. 10e.

5.4. Model validation with a literature dataset

In this section the bearing capacity predictions of the GPC-model are validated using a literature dataset containing 57 external experiments and 22 experiments conducted at TU Wien previously discussed in Section 4. The range of the investigated parameters compared to the presented experimental campaign can therefore be extended to different geometries (rectangular shapes) of the test specimens and reinforcement layouts, as well as a wide range of mechanical reinforcement ratios ω (0.008–0.470) and load concentration ratios A_{cc}/A_{c0} (1.18 - 9.0). For the application of the GPC-model to rectangular shaped

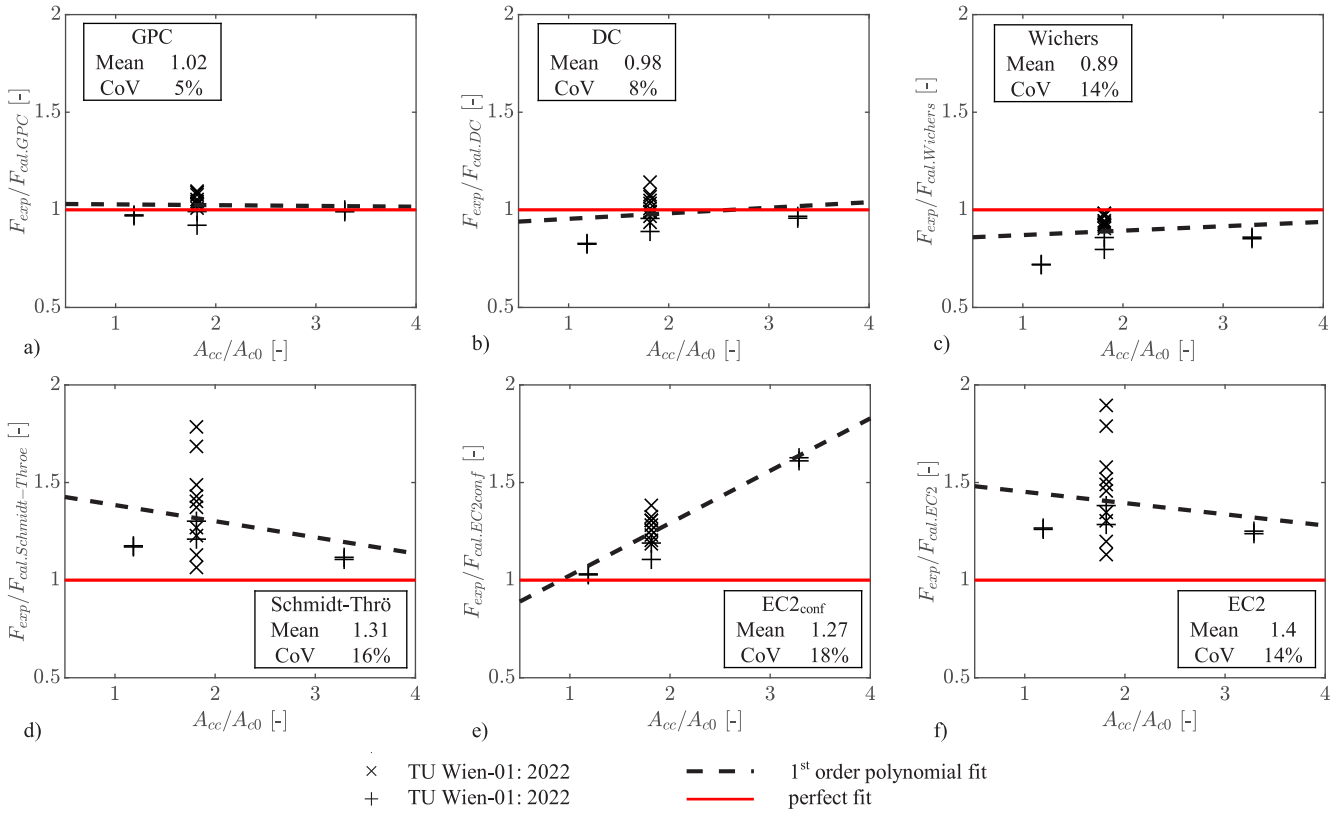

Fig. 10. Ratio of experimental and predicted load-bearing capacities using different models from literature as a function of the load distribution ratio A_{cc}/A_{c0} within (a) $F_{cal.GPC}$ according to Eq. (9), (b) following the flowchart according to Fig. 7 on page 13 in Markić et al. [4], (c) $F_{cal.Wichers}$ according to Eq. (8), (d) $F_{cal.Schmidt-Thrö}$ according to Eq. (7), (e) $F_{cal.EC2conf}$ according to Eq. (3), (f) $F_{cal.EC2}$ according to Eq. (2). (For interpretation of the references to color in this figure, the reader is referred to the web version of this article.).

elements the passive confinement was determined following the procedure according to [22] which is based on the EC2-draft [1]. The whole dataset containing experimental results from Wurm & Daschner [16], Bonetti [20] and Ahmed [33] is enclosed in Appendix B.

Beside the spatial load distribution and the impediment of lateral expansion by reinforcement, other parameters like the slenderness of the specimens, an insufficient reinforcement layout and the load introduction system may influence the load-bearing capacity of concrete elements. To make sure that the two investigated effects are responsible for the reached load-bearing capacity, the following criteria have to be met by the test specimen design to be selected for the validation:

- The specimens have to be loaded centrically.
- Geometric and passive confinement effects must be fully activated when reaching the failure load, meaning section 0–0, according to Fig. 3, should be decisive for failure.
- Therefore the test specimens have to include a minimum mechanical transverse reinforcement ratio ω and
- the geometrical requirement $A_{c0} < A_{cc}$ has to be fulfilled to enable the passive confinement effect.
- Detailed information about mechanical and geometrical properties have to be available, to exclude an early failure in region R_1 according to Fig. 3.
- To exclude side effects in the discontinuity area next to the contact surface the ratio of H/d (according to Fig. 5) has to be at least 1.5.

Test datasets derived from literature meeting all the above mentioned criteria are rare. If tests which were performed with steel plates for load introduction were additionally excluded, no meaningful validation would be possible. Therefore, the influence of the load application is investigated in Section 5.5.

The dataset summarized by Wichers [15] gives a good overview on previously performed tests regarding concentrated load applications in concrete structures. The well known experiments of Niyogi [17] are, however, excluded from this paper due to the ratio of H/d only amounting to 1.0. Furthermore, for the dataset of Bonetti [20] detailed information regarding the location and the amount of reinforcement is missing.

In Fig. 12 the ratio of the experimental and calculated bearing capacities is plotted as a function of the transverse mechanical ratio. The optimum for a prediction is represented by the horizontal red line.

The experimental data was underestimated with the mean ratio of F_{exp}/F_{GPC} of 1.19 (shown in Fig. 12). One reason for the inaccuracy could be the load introduction systems used in literature. As shown in Section 5.5, using a steel plate can lead to an underestimation of up to 6.5 % for moderate confined specimens. Another reason might be the missing geometrical data of the experiments from literature. The spacing between the contact surface and the first transverse reinforcement layer $s_{c.cont}$, for example, had to be estimated with $s_c/2$ (see Table B.1) within the calculations using the GPC-model. If the distance in reality was smaller than assumed, the load-bearing capacity could exceed the prediction of the GPC-model.

The DC-model, was the only one which performed on the same level of accuracy applied to the experiments presented in this paper (shown in Fig. 10). The literature validation of the Dual Cone-model in Markić et al. [26] resulted in a mean ratio between F_{exp}/F_{DC} of 1.32 and a variation coefficient of 32 %, which is slightly more inaccurate than the validation of the GPC-model with the values of 1.16 and 13 %.

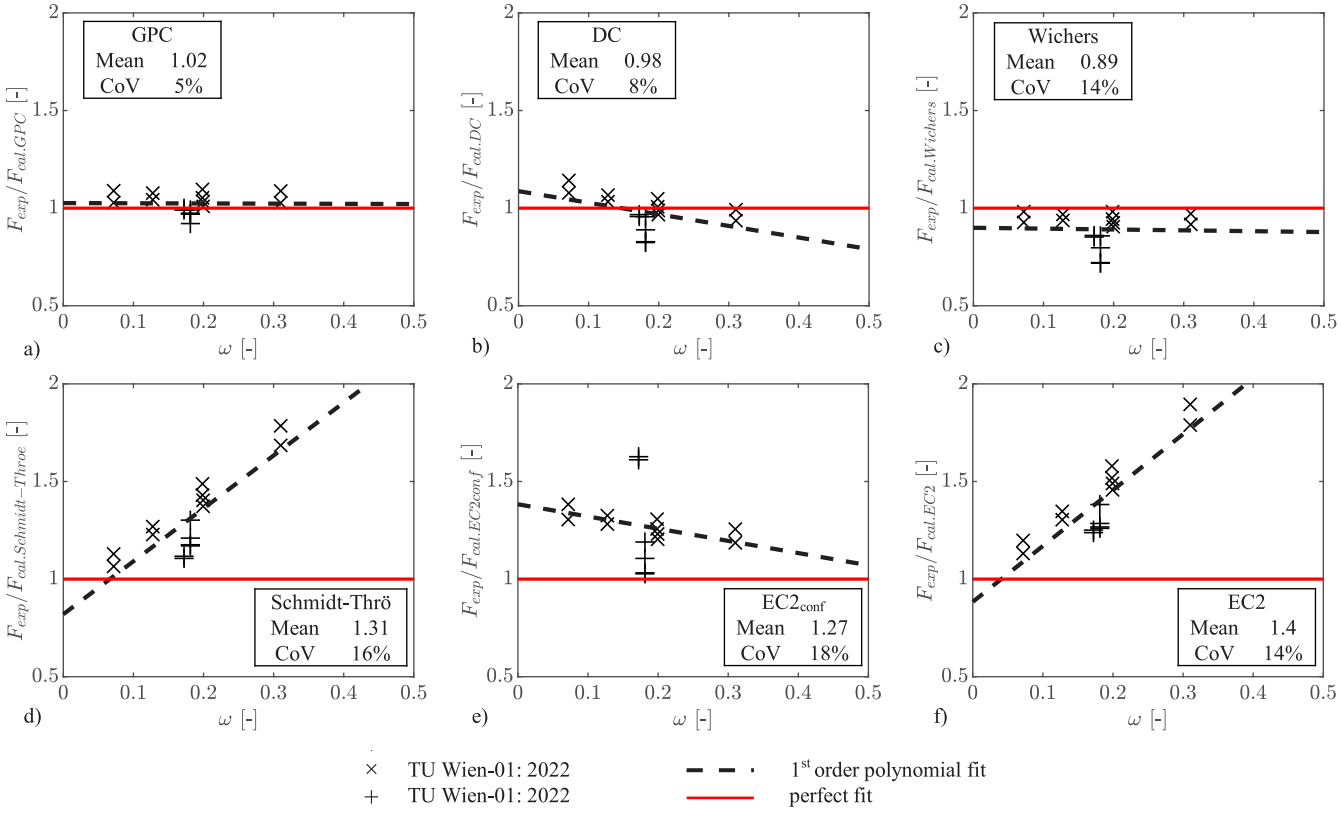

Fig. 11. Ratio of experimental and predicted load-bearing capacities using different models from literature as a function of the transverse mechanical reinforcement ratio ω within (a) $F_{cal.GPC}$ according to Eq. (9), (b) following the flowchart according to Fig. 7 on page 13 in Markić et al. [4], (c) $F_{cal.Wichers}$ according to Eq. (8), (d) $F_{cal.Schmidt-Thrö}$ according to Eq. (7), (e) $F_{cal.EC2conf}$ according to Eq. (3), (f) $F_{cal.EC2}$ according to Eq. (2). (For interpretation of the references to color in this figure, the reader is referred to the web version of this article.).

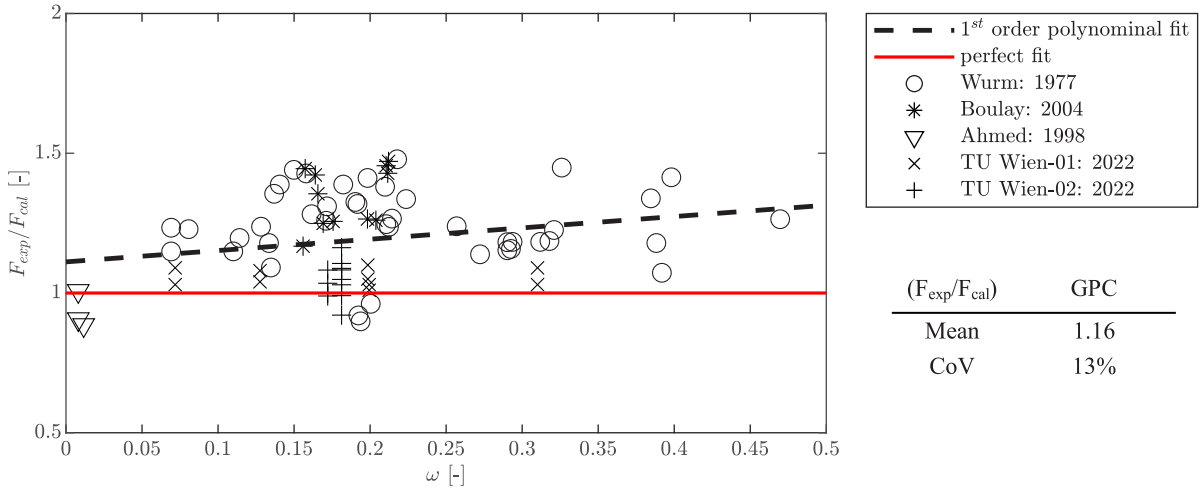

Fig. 12. Ratio of experimental and predicted load-bearing capacities as a function of the transverse mechanical reinforcement ratio ω [-] for the GPC-model. (For interpretation of the references to color in this figure, the reader is referred to the web version of this article.).

5.5. Relevance of the load introduction system

Table 3 provides an overview of the peak loads and derived mean values of the test specimens which were accessed to investigate the influence of the load introduction system. When compared to a more realistic setting where load transmission occurs between two concrete elements, specimens examined with a load applied to a steel plate led to higher peak loads, increasing by 4.5 % for specimen type I2 and 6.5 % for K2. For a detailed discussion regarding the differences of the load–strain curves and the contact surface failures the authors refer to [34].

As all tested specimens had the same reinforcement layout, it is not possible to assign the results to specimens with reinforcement ratios different to $\rho = 1.65\,\%$ without a degree of uncertainty. However, it is

Table 3
Comparison of peak loads F_{exp} [in kN] regarding c–c (concrete–concrete) and st–c (steel plate–concrete) load introduction.

Specimen type	I2	I2a	K2	K2a
Load transfer	c – c	st – c	c – c	st – c
F_{exp}–V1	980	1052	614	665
F_{exp}–V2	985	1001	608	636
F_{exp}–average	983	1027	611	651
	100 %	104.5 %	100 %	106.5 %

to be expected that the impact of the load introduction system increases for unreinforced specimens and decreases for reinforced specimens as the reinforcement ratio increases. With regard to the validation with the literature dataset, where all the tests were conducted with steel plates, an inaccuracy of about 4.5 %–6.5 % for moderate passively confined specimens is seen as acceptable. This might be an explanation for the slight underestimation of the GPC-model in comparison to the experimental failure loads compared in Fig. 12.

5.6. Suggestions for a practical design of a load transfer zone

Based on the experimental campaign and the proposed GPC-model the following suggestions for a practical design of a load transfer zone are given:

- A minimum transverse reinforcement ratio is required to avoid a brittle failure and enable geometric and post-cracking passive confinement. It is recommended to set the minimum at $\rho = 0.5\,\%$. For reinforcement with a lower yield strength or a higher concrete strength than used in the experiments a minimum mechanical transverse reinforcement ratio of $\omega = 6\,\%$ must be provided.
- There need to be at least two reinforcement layers inside the discontinuity region to provide passive confinement in R_0 and to cover the tensile stresses in R_1.
- The first transverse reinforcement element has to be located at a distance $\leq 0.5 \cdot s_c$ from the contact surface to guarantee a passive confinement effect of the reinforcement.
- The last transverse reinforcement should be positioned $\geq 0.9 \cdot h$ from the contact surface, to provide passive confinement along the entire discontinuity region and to avoid an overlap of transverse tensile stresses caused by the load distribution [27] and the transition zone.
- The spacing s_c between the reinforcement layers in the discontinuity region has to be constant.
- If the ratio of the area available for load distribution and the contact surface A_{cc}/A_{c0} gets too large, a reduction of the passive confinement effect can be expected. According to the EC2-draft [1] the confinement has to be reduced by a factor when A_{cc} is more than twice A_{c0}. The experimental campaign presented in this paper covers a maximum ratio between A_{cc}/A_{c0} of 3.3, resulting in the authors' recommendation to set the A_{cc}/A_{c0} ratio at a maximum of 3.3 for a feasible application of the GPC-model.

6. Conclusions

The goal of this research was to investigate the load-bearing behavior of load transfer zones regarding their specific boundary conditions of small ratios of A_{cc}/A_{c0} (1.0–3.29), high transverse reinforcement ratios (up to 2.57 %) and concrete–concrete (c–c) load introduction such as can be found in the longitudinal joint of tunnel segments. In a systematic experimental campaign the load-bearing behavior of geometric and passive confinement in load transfer zones was investigated. The following conclusions can be drawn regarding the conducted experiments:

- Both, the transverse reinforcement ratio (passive confinement) and the load distribution, which causes geometric confinement, have a significant influence on the compressive stresses in the contact surface when reaching the peak load (Fig. 8).
- It was found that only the passive confinement has a significant influence on the ductility of the load transfer zone (Table 2).
- Both design approaches of the EC2-draft [1] yield inaccurate results depending on the reinforcement and the load concentration ratio (Fig. 8).
- The use of steel plates for load introduction of moderately passively confined specimens leads to an increase of the load-bearing capacity of about 4.5 %–6.5 % compared to the concrete to concrete load transfer.

The authors present a mechanical approach for more accurate prediction of the load-bearing capacity for geometric and passive confinement in load transfer zones. The Geometric and Passive Confinement-model (GPC-model) is built on a mechanical basis and complemented by a semi-empirical component to capture the effects of load distribution and confinement reinforcement. While some models have been established that cover the geometric and passive confinement effects only individually and some models permit a combination but with several limitations or a high computational effort, this work provides a solution that accounts for both effects without these limitations. Due to its simple analysis procedure it has the potential to be widely applied by practitioners in the future. In comparison to most existing models, it covers failure mechanisms along the entire discontinuity region (simplified in two sections as outlined in Fig. 3), which ensures a safe design and enables resource-efficient reinforcement layouts for load transfer zones. Due to the mechanical basis, the GPC-model can be adapted for more complex geometries and reinforcement layouts (e.g. the longitudinal joint between two tunnel segments). A detailed transition of the proposed model for tunnel segments and a verification with an experimental campaign on longitudinal joints of tunnel segments will be shown in upcoming publications.

CRediT authorship contribution statement

Clemens Proksch-Weilguni: Writing – original draft, Validation, Methodology, Investigation, Conceptualization. **Marion Decker:** Writing – review & editing, Methodology, Investigation. **Johann Kollegger:** Writing – review & editing, Supervision, Funding acquisition.

Declaration of competing interest

The authors declare that they have no known competing financial interests or personal relationships that could have appeared to influence the work reported in this paper.

Data availability

Data will be made available on request.

Acknowledgment

The authors acknowledge the support of:

- The TU Wien Bibliothek for financial support through its Open Access Funding Programme.
- The staff of the Institute of Structural Engineering laboratory at TU Wien for the help during the experiments: Dr. Wolfgang Träger, Klemens Wagner, Dipl.-Ing. Herbert Pardatscher and Hannes Fleischhacker.
- Dr. Johannes Kirnbauer for his efforts and expertise in preparing the concrete mixtures.
- Fabian Morger, MSc for his support regarding the application of the DC-model.

Appendix A. Load–strain curves

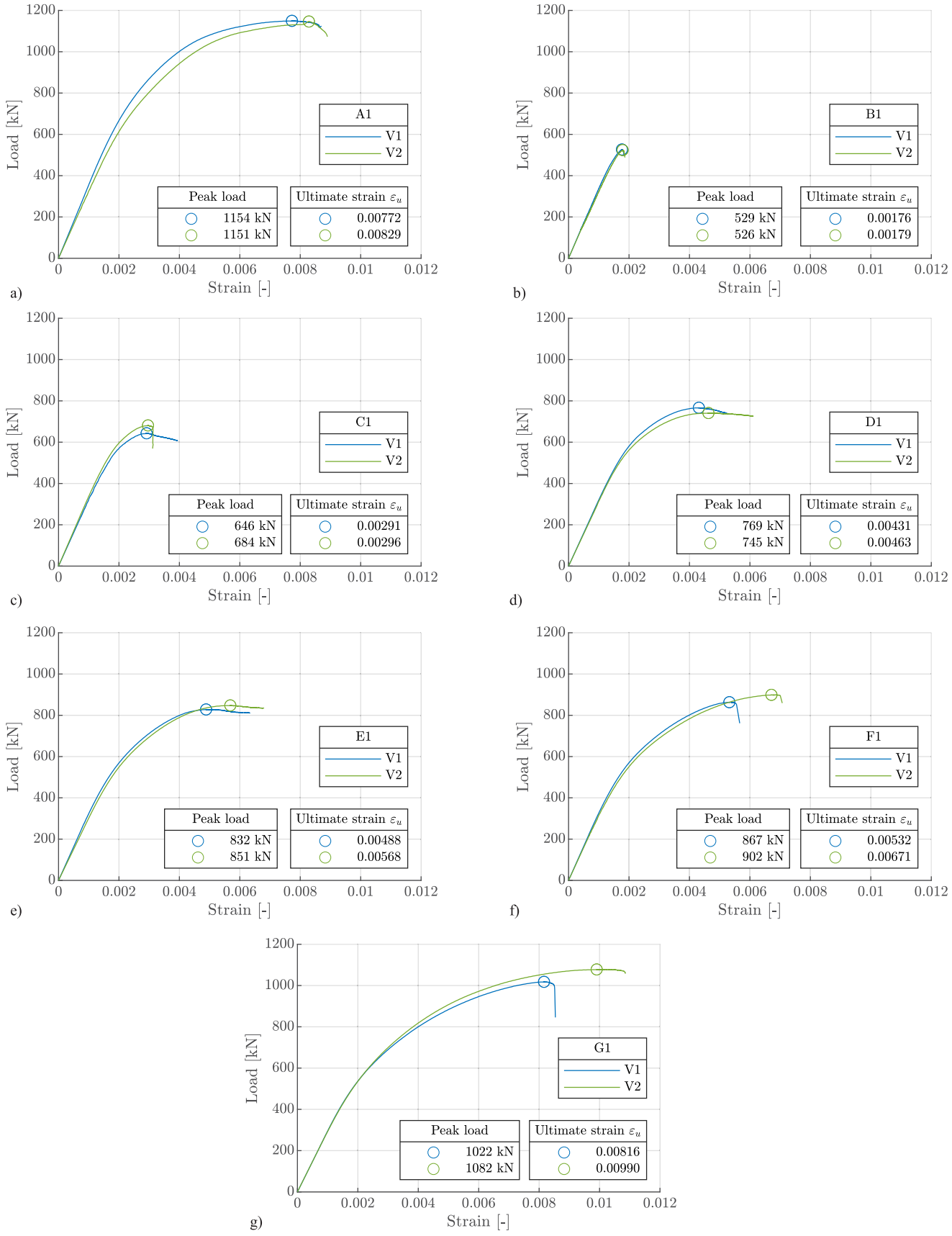

Fig. A.1. Load–strain curves of the experiments conducted at TU Wien.

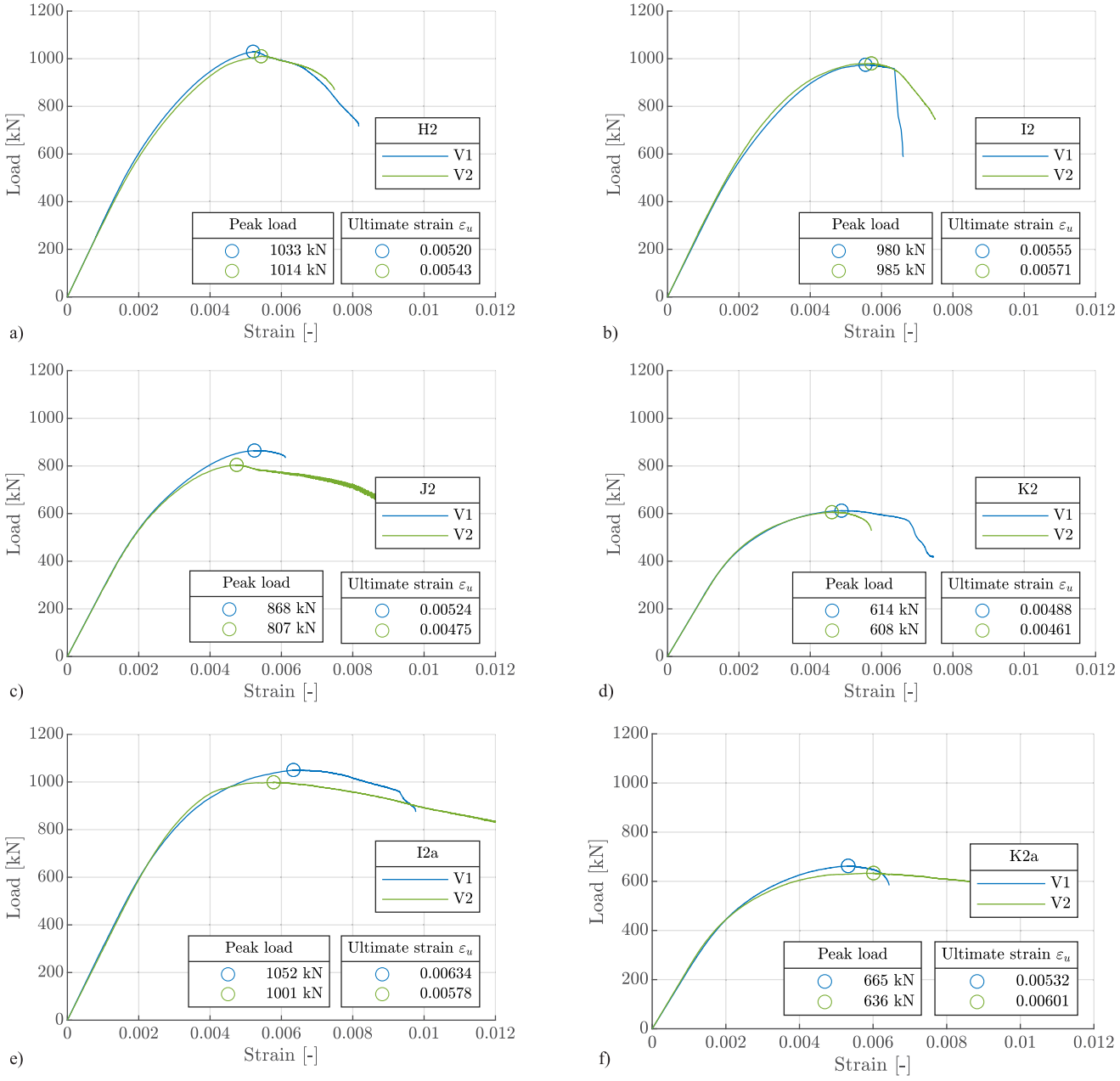

Fig. A.2. Load–strain curves of the experiments conducted at TU Wien.

Appendix B. Dataset

Table B.1
Experiments used to validate the GPC-model.

General information		Concrete specimen			Reinforcement						Material properties		Results		
Source	Name	b_1; d_1 [mm]	H [mm]	b_0; d_0 [mm]	s_c [mm]	$s_{c.cont}$ [mm]	b_c; d_c [mm]	ø[mm]	ρ	ω	f_{cm} [N/mm²]	f_{ym} [N/mm²]	F_{exp} [kN]	σ_{c0}/ f_{cm}	F_{exp}/ $F_{cal.GPC}$
Wurm & Daschner [16]	16 (III D)	300	600	150	42	–	270	10	0.0139	0.1983	26.1	374	1980.0	3.37	1.41
	22 (III D)	300	600	150	42	–	270	10	0.0139	0.1903	27.2	374	1912.0	3.12	1.33
	28 (III D)	300	600	150	42	–	270	10	0.0139	0.1917	27.0	374	1892.0	3.11	1.32
	18 (III F)	300	600	150	60	30	270	12	0.0140	0.2004	26.1	375	1402.4	2.39	0.92
	24 (III F)	300	600	150	60	30	270	12	0.0140	0.1923	27.2	375	1382.7	2.26	0.88
	30 (III F)	300	600	150	60	30	270	12	0.0140	0.1937	27.0	375	1343.5	2.21	0.86
	15 (III C)	300	600	150	51	–	270	12	0.0164	0.1710	27.5	286	1775.0	2.87	1.26
	21 (III C)	300	600	150	51	–	270	12	0.0164	0.1717	27.4	286	1843.0	2.99	1.31
	27 (IIIC)	300	600	150	51	–	270	12	0.0164	0.1823	25.8	286	1873.0	3.23	1.39
	13 (III A)	300	600	150	41	–	270	12	0.0204	0.2099	27.5	282	2079.0	3.36	1.38
	19 (III A)	300	600	150	41	–	270	12	0.0204	0.2106	27.4	282	1873.0	3.04	1.25
	25 (III A)	300	600	150	41	–	270	12	0.0204	0.2237	25.8	282	1931.0	3.33	1.34
	14 (III B)	300	600	150	46	–	270	14	0.0248	0.2926	27.5	325	1981.0	3.20	1.16
	20 (III B)	300	600	150	46	–	270	14	0.0248	0.2937	27.4	325	2020.0	3.28	1.18
	26 (III B)	300	600	150	46	–	270	14	0.0248	0.3119	25.8	325	1952.0	3.36	1.18
	36 (IV B)	300	600	150	50	–	270	8	0.0074	0.0806	25.9	280	1373.0	2.36	1.23
	37 (IV B)	300	600	150	50	–	270	8	0.0074	0.0692	30.2	280	1461.0	2.15	1.15
	38 (IV B)	300	600	150	50	–	270	8	0.0074	0.0692	30.2	280	1569.0	2.31	1.23
	35 (IV B)	300	600	150	51	–	270	10	0.0114	0.1283	25.9	291	1520.0	2.61	1.24
	39 (IV B)	300	600	150	51	–	270	10	0.0114	0.1100	30.2	291	1589.0	2.34	1.15
	40 (IV B)	300	600	150	51	–	270	10	0.0114	0.1142	29.1	291	1608.0	2.46	1.20
	33 (IV B)	300	600	150	49	–	270	12	0.0171	0.1499	27.3	239	1942.0	3.16	1.44
	34 (IV B)	300	600	150	49	–	270	12	0.0171	0.1580	25.9	239	1853.0	3.18	1.43
	41 (IV B)	300	600	150	49	–	270	12	0.0171	0.1406	29.1	239	1961.0	3.00	1.39
	31 (IV B)	300	600	150	47	–	270	16	0.0317	0.2903	27.3	250	2001.0	3.26	1.18
	32 (IV B)	300	600	150	47	–	270	16	0.0317	0.2903	27.3	250	1952.0	3.18	1.15
	42 (IV B)	300	600	150	47	–	270	16	0.0317	0.2723	29.1	250	2001.0	3.06	1.14
	115 (XIII)	300	600	150	42	–	270	8	0.0089	0.1615	26.7	486	1726.0	2.87	1.28
	116 (XIII)	300	600	150	42	–	270	8	0.0089	0.1348	32.0	486	1677.0	2.33	1.09
	117 (XIII)	300	600	150	42	–	270	8	0.0089	0.1335	32.3	486	1824.0	2.51	1.18
	119 (XIII)	300	600	150	42	–	270	10	0.0139	0.2569	26.7	495	1952.0	3.25	1.24
	120 (XIII)	300	600	150	42	–	270	10	0.0139	0.2144	32.0	495	2236.0	3.11	1.27
	121 (XIII)	300	600	150	42	–	270	10	0.0139	0.2124	32.3	495	2197.0	3.02	1.24
	123 (XIII)	300	600	150	42	–	270	12	0.0199	0.3846	26.7	515	2520.0	4.19	1.34
	124 (XIII)	300	600	150	42	–	270	12	0.0199	0.3209	32.0	515	2540.0	3.53	1.23
	125 (XIII)	300	600	150	42	–	270	12	0.0199	0.3179	32.3	515	2471.0	3.40	1.19
	127 (XIII)	300	600	150	42	–	270	14	0.0271	0.4697	26.7	462	2638.0	4.39	1.26
	128 (XIII)	300	600	150	42	–	270	14	0.0271	0.3919	32.0	462	2442.0	3.39	1.07
	129 (XIII)	300	600	150	42	–	270	14	0.0271	0.3882	32.3	462	2697.0	3.71	1.18
	118 (XIV)	300	600	100	42	–	270	8	0.0089	0.1369	31.5	486	1255.0	3.98	1.35
	122 (XIV)	300	600	100	42	–	270	10	0.0139	0.2178	31.5	495	1520.0	4.83	1.48
	126 (XIV)	300	600	100	42	–	270	12	0.0199	0.3260	31.5	515	1687.0	5.36	1.45
	130 (XIV)	300	600	100	42	–	270	14	0.0271	0.3981	31.5	462	1775.0	5.63	1.41
Bonetti [20]	1 (C50)	200	600	100	38	–	152	8	0.0174	0.1691	56.6	550	1241.0	2.19	1.14
	2 (C50)	200	600	100	38	–	152	8	0.0174	0.1756	54.5	550	1208.0	2.22	1.15
	2 (C50)	200	600	100	38	–	152	8	0.0174	0.1559	61.4	550	1245.0	2.03	1.07
	4 (C70)	200	600	100	33	–	152	10	0.0313	0.2121	81.2	550	2195.0	2.70	1.33
	5 (C70)	200	600	100	33	–	152	10	0.0313	0.2116	81.4	550	2136.0	2.62	1.29
	6 (C70)	200	600	100	33	–	152	10	0.0313	0.2106	81.8	550	2185.0	2.67	1.31
	7 (C105)	200	600	100	43	–	152	12	0.0346	0.1657	114.9	550	2699.0	2.35	1.24
	8 (C105)	200	600	100	43	–	152	12	0.0346	0.1639	116.1	550	2859.0	2.46	1.30
	9 (C105)	200	600	100	43	–	152	12	0.0346	0.1573	121.0	550	3012.0	2.49	1.33
	10 (C110)	200	600	100	32	–	152	12	0.0465	0.1983	129.0	550	2972.0	2.30	1.15
	11 (C110)	200	600	100	32	–	152	12	0.0465	0.2038	125.5	550	2895.0	2.31	1.14
Ahmed [33]	R2 - C	200	300	50	50	–	150	2.5	0.0013	0.0081	47.0	290	359.0	3.06	1.01
	R2 - C	200	300	50	50	–	150	2.5	0.0013	0.0081	47.0	290	459.0	1.95	0.91
	R2 - C	400	600	100	100	–	300	6	0.0019	0.0116	47.0	290	1268.0	2.70	0.89
TU Wien (this paper)	A1-V1	150	300	150	45	22.5	136	8	0.0164	0.1985	48.0	580	1154.0	1.36	1.07
	A1-V2	150	300	150	45	22.5	136	8	0.0164	0.1985	48.0	580	1151.0	1.36	1.06
	C1-V1	150	300	101	70	35	136	6	0.0059	0.0718	48.0	580	645.8	1.68	1.03
	C1-V2	150	300	101	70	35	136	6	0.0059	0.0718	48.0	580	684.3	1.78	1.09
	D1-V1	150	300	101	70	35	136	8	0.0106	0.1276	48.0	580	769.4	2.00	1.08
	D1-V2	150	300	101	70	35	136	8	0.0106	0.1276	48.0	580	744.5	1.94	1.04
	E1-V1	150	300	101	70	35	136	10	0.0165	0.1994	48.0	580	832.3	2.16	1.01
	E1-V2	150	300	101	70	35	136	10	0.0165	0.1994	48.0	580	851.0	2.21	1.03
	F1-V1	150	300	101	45	22.5	136	8	0.0164	0.1985	48.0	580	867.0	2.25	1.05
	F1-V2	150	300	101	45	22.5	136	8	0.0164	0.1985	48.0	580	902.0	2.35	1.10
	G1-V1	150	300	101	45	22.5	136	10	0.0257	0.3101	48.0	580	1021.6	2.66	1.03
	G1-V2	150	300	101	45	22.5	136	10	0.0257	0.3101	48.0	580	1082.1	2.81	1.09

(*continued on next page*)

Table B.1 (*continued*).

General information		Concrete specimen			Reinforcement						Material properties		Results		
Source	Name	b_1; d_1 [mm]	H [mm]	b_0; d_0 [mm]	s_c [mm]	$s_{c,cont}$ [mm]	b_c; d_c [mm]	ø[mm]	ρ	ω	f_{cm} [N/mm^2]	f_{ym} [N/mm^2]	F_{exp} [kN]	σ_{c0}/f_{cm}	$F_{exp}/F_{cal.GPC}$
TU Wien (this paper)	H2-V1	150	300	150	70	35	136	10	0.0165	0.1812	52.8	580	1033.0	1.11	0.96
	H2-V2	150	300	150	70	35	136	10	0.0165	0.1812	52.8	580	1014.0	1.09	0.94
	I2-V1	150	300	125	70	35	136	10	0.0165	0.1812	52.8	580	980.0	1.51	0.97
	I2-V2	150	300	125	70	35	136	10	0.0165	0.1812	52.8	580	985.0	1.52	0.97
	J2-V1	150	300	101	70	35	136	10	0.0165	0.1812	52.8	580	868.0	2.05	0.99
	J2-V2	150	300	101	70	35	136	10	0.0165	0.1812	52.8	580	807.0	1.91	0.92
	K2-V1	150	300	75	70	35	136	10	0.0165	0.1721	55.6	580	614.0	2.50	1.00
	K2-V2	150	300	75	70	35	136	10	0.0165	0.1721	55.6	580	608.0	2.48	0.99
	I2a-V1	150	300	125	70	35	136	10	0.0165	0.1812	52.8	580	1052.0	1.62	1.04
	I2a-V2	150	300	125	70	35	136	10	0.0165	0.1812	52.8	580	1001.0	1.54	0.99
	K2a-V1	150	300	75	70	35	136	10	0.0165	0.1721	55.6	580	665.0	2.71	1.08
	K2a-V2	150	300	75	70	35	136	10	0.0165	0.1721	55.6	580	636.0	2.59	1.03

References

[1] ÖNORM FprEN 1992-1-1: Design of concrete structures - Part 1-1: General rules - Rules for buildings, bridges and civil engineering structures; FprEN 1992-1-1:2023. Brussels: European Commitee for Standardization; 2023.

[2] Saint-Venant A. Memoire sur la torsion des prismes: avec des considérations sur leur fléxion ainsi que sur l'équilibre intérieur des solides élastiques en général, et des formules pratiques pour le calcul de leur résistance à divers efforts s'exerçant simultanément. Paris: Imprimerie Nationale; 1856.

[3] Markić T, Kaufmann W, Amin A. Stress field solution for strip loaded reinforced concrete blocks. Engineering Structures 2018;171:911–20. http://dx.doi.org/10.1016/j.engstruct.2018.03.027.

[4] Markić T, Morger F, Kaufmann W. Partially loaded areas in reinforced concrete: Mechanical modelling. Engineering Structures 2022;271:114938. http://dx.doi.org/10.1016/j.engstruct.2022.114938.

[5] Bauschinger J. Versuche mit Quadern aus Naturstein. In: Mitteilungen aus dem Mechanisch Technischen Laboratorien der Technischen Hochschule München. Vol. 6. 1876, p. 1–20.

[6] ÖNORM EN 1992-1-1: Design of concrete structures: Part 1-1: General rules and rules for buildings. Vienna: Austrian Standards Institute; 2015.

[7] fib: Model code for concrete structures 2010. Lausanne: International Federation for Structural Concrete (fib); 2013.

[8] SIA 262: Betonbau. Zürich: Schweizerischer Ingenieur- und Architektenverein; 2013.

[9] Spieth H-P. Das Verhalten von Beton unter hoher örtlicher Pressung und Teilbelastung unter besonderer Berücksichtigung von Spannbetonverankerungen (Ph.D. thesis), Technische Hochschule Stuttgart; 1959.

[10] Fardis MN. Seismic design, assessment and retrofitting of concrete buildings: based on EN-Eurocode. Vol. 8. Springer Science & Business Media; 2009, http://dx.doi.org/10.1007/978-1-4020-9842-0.

[11] Richart FE, Brandtzaeg A, Brown RL. Failure of plain and spirally reinforced concrete in compression. University of Illinois. Engineering Experiment Station; 1929, Bulletin no. 190.

[12] Mander JB, Priestley MJN, Park R. Theoretical stress and strain model for confined concrete. Journal of Structural Engineering 1988;114(8):1804–26. http://dx.doi.org/10.1061/(ASCE)0733-9445(1988)114:8(1804).

[13] Spieth H-P. Das Verhalten von Beton unter hoher örtlicher Pressung. Beton- und Stahlbetonbau 1961;56(Heft 11):257–62.

[14] DAUB: Empfehlungen für den Entwurf, die Herstellung und den Einbau von Tübbingringen. Köln: Deutscher Ausschuss für unterirdisches Bauen; 2013.

[15] Wichers M. Bemessung von bewehrten Betonbauteilen bei Teilflächenbelastung unter Berücksichtigung der Rissbildung (Ph.D. Thesis), Technische Universität Braunschweig; 2013.

[16] Wurm P, Daschner F. Versuche Über Teilflächenbelastung Von Normalbeton (DAfStb Heft 286). Deutscher Ausschußfür Stahlbeton, Verlag von Wilhelm Ernst & Sohn, Technische Univeristät München; 1977.

[17] Niyogi SK. Bearing strength of reinforced concrete blocks. Journal of the Structural Division 1975;101(5):1125–37. http://dx.doi.org/10.1061/JSDEAG.0004053.

[18] Schmidt-Thrö G. Zum Tragverhalten der Tübbinglängsfuge (Ph.D. thesis), Technische Universität München; 2019, URL http://mediatum.ub.tum.de/node?id=1484068.

[19] Wurm P, Daschner F. Teilflächenbelastung Von Normalbeton Versuche an Bewehrten Scheiben (DAfStb Heft 344). Deutscher Ausschuß für Stahlbeton, Verlag von Wilhelm Ernst & Sohn; 1983.

[20] Bonetti RA. Ultimate strength of the local zone in load transfer tests (Ph.D. thesis), Virginia Polytechnic Institute and State University; 2005.

[21] Empelmann M, Wichers M. Stabwerke und Teilflächenbelastung nach DIN 1045-1 und Eurocode 2 – Modelle und Anwendungen. Beton- und Stahlbetonbau 2009;104(4):226–35. http://dx.doi.org/10.1002/best.200900668.

[22] Proksch-Weilguni C, Decker M, Kollegger J. Hochbelastete Lastübertragungszonen mit stumpf gestoßener Bewehrung: Experimentelle Untersuchungen und numerische Simulationen. Beton- und Stahlbetonbau 2022;117(11):913–27. http://dx.doi.org/10.1002/best.202200075.

[23] Mörsch E. Über die Berechnung der Gelenkquader. Beton und Eisen 1924;23(12):156–61.

[24] Schmidt-Thrö G, Tabka B, Smarslik M, Scheufler W, Fischer O, Mark P. Experimente zur Teilflächenpressung mit vorwiegend ebener Lastausbreitung. Beton- und Stahlbetonbau 2018;113(2):115–26. http://dx.doi.org/10.1002/best.201700081.

[25] Schmidt-Thrö G, Smarslik M, Tabka B, Scheufler W, Fischer O, Mark P. Experimental analysis of concrete elements under partial area strip loading. Civil Engineering Design 2019;1(1):28–38. http://dx.doi.org/10.1002/cend.201900001.

[26] Markić T, Morger F, Kaufmann W. Partially loaded areas in reinforced concrete: Experimental campaign and model validation. Engineering Structures 2022;273:114905. http://dx.doi.org/10.1016/j.engstruct.2022.114905.

[27] DAfStb-Heft 631: Hilfsmittel zur Schnittgrößenermittlung und zu besonderen Detailnachweisen bei Stahlbetontragwerken. Berlin: Beuth Verlag GmbH; 2019, 2019.

[28] Iyengar KTSR. Der Spannungszustand in einem elastischen Halbstreifen und seine technischen Anwendungen (Ph.D. thesis), TH Hannover; 1960.

[29] Yettram AL, Robbins K. Anchorage zone stresses in post-tensioned uniform members with eccentric and multiple anchorages. Magazine of Concrete Research 1970;22(73):209–18. http://dx.doi.org/10.1680/macr.1970.22.73.209.

[30] Sigrist V. Zum Verformungsvermögen von Stahlbetonträgern (Ph.D. thesis), Eidgenössische Technische Hochschule Zürich; 1995, http://dx.doi.org/10.3929/ethz-a-001492371.

[31] ONR 23303: 2010 09 01: Prüfverfahren Beton (PVB) – Nationale Anwendung der Prüfnormen für Beton und seiner Ausgangsstoffe. Wien: Austrian Standards; 2010.

[32] Meusburger. Technical data sheet tool steel 1.2312. 2023, https://www.meusburger.com/DE/DE/materialqualitaeten/12312-werkzeugstahl. [Accessed 08 May 2023].

[33] Ahmed T, Burley E, Rigden S. Bearing capacity of plain and reinforced concrete loaded over a limited area. ACI Structural Journal 1998;95(3). http://dx.doi.org/10.14359/550.

[34] Decker M, Proksch-Weilguni C, Kollegger J. Load transfer in tunnel segments: A contribution to emphasize the importance of the load introduction system in experimental testing. In: Ilki A, Çavunt D, Çavunt YS, editors. Fib symposium 2023. Springer Nature Switzerland; p. 1745–51. http://dx.doi.org/10.1007/978-3-031-32511-3_179.